Non-covalent lanthanide podates with predetermined physicochemical properties: iron(II) spin-state equilibria in self-assembled heterodinuclear d–f supramolecular complexes †

Claude Piguet,[*,a] **Elisabeth Rivara-Minten,**[a] **Gérald Bernardinelli,**[b] **Jean-Claude G. Bünzli**[*,c] **and Gérard Hopfgartner**[d]

[a] *Department of Inorganic, Analytical and Applied Chemistry, University of Geneva, 30 quai E. Ansermet, CH-1211 Geneva 4, Switzerland*

[b] *Laboratory of X-Ray Crystallography, 24 quai E. Ansermet, CH-1211 Geneva 4, Switzerland*

[c] *Institute of Inorganic and Analytical Chemistry, University of Lausanne, BCH 1402, CH-1015 Lausanne-Dorigny, Switzerland*
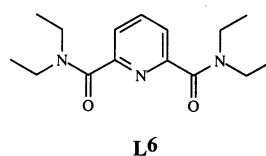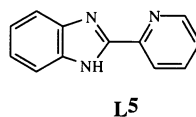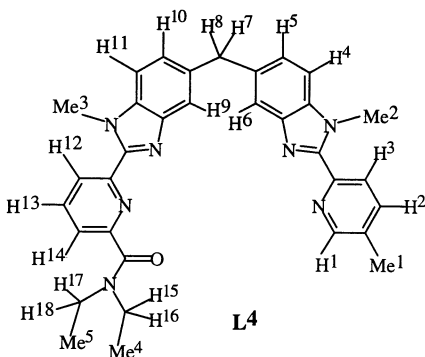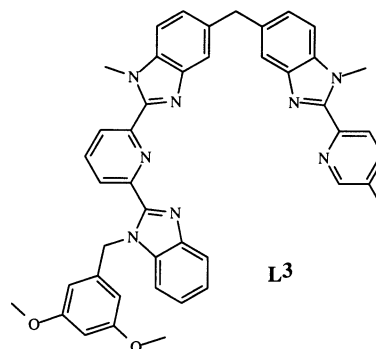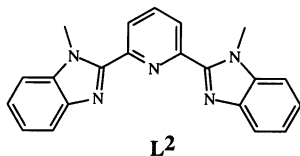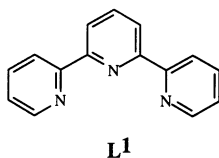
[d] *F. Hoffmann-La Roche Ltd., Pharmaceuticals Division, Department of Drug Metabolism and Kinetics, CH-4070 Basle, Switzerland*

The reaction of the segmental compound 2-[6-(diethylcarbamoyl)pyridin-2-yl]-1,1′-dimethyl-2′-(5-methylpyridin-2-yl)-5,5′-methylenebis(1H-benzimidazole) (L) with a stoichiometric mixture of Fe^{II} and Ln^{III} (Ln = La, Nd, Eu, Gd, Tb, Yb, Lu, Y or Sc) or Ca^{II} in acetonitrile produced selectively the heterodinuclear non-covalent podates [LnFeL$_3$]$^{5+}$ and [CaFeL$_3$]$^{4+}$. Proton NMR and electronic spectroscopy and electrochemistry showed that the ligands are helically wrapped around the metal ions leading to a C_3-triple-helical structure with Fe^{II} occupying the pseudo-octahedral co-ordination site produced by the three bidentate binding units and Ln^{III} lying in the remaining pseudo-tricapped trigonal-prismatic site defined by the three tridentate binding units. In this chemical environment Fe^{II} sustains a thermally induced low-spin $\longrightarrow$ high-spin transition around room temperature in acetonitrile, the thermodynamic parameters of which can be finely controlled by the size of the co-ordinated Ln^{III}. Thermodynamic investigations of the assembly process suggest that the stability of the final complexes [LnFeL$_3$]$^{5+}$ depends on the size of Ln^{III}, small metal ions leading to intricate mixtures of complexes. The crystal structure of [LaFeL$_3$][ClO$_4$]$_{0.5}$[CF$_3$SO$_3$]$_{4.5}$·MeCN·4H$_2$O at 170 K is isostructural with that of [EuZnL$_3$][ClO$_4$][CF$_3$SO$_3$]$_4$·4MeCN and indicates that (*i*) the Fe–N bonds are in the range expected for essentially low-spin Fe^{II} and (*ii*) [LaFeL$_3$]$^{5+}$ adopts the regular triple-helical structure found in solution. Magnetic measurements in the solid state showed smooth spin transitions similar to those observed in solution, while photophysical studies suggested that Eu^{III}→Fe^{II} (low-spin) energy transfers are responsible for the complete quenching of the Eu-centred emission.

The importance of the lanthanide metal ions, Ln^{III}, mainly results from the peculiar spectroscopic and magnetic properties associated with their 4f^n electronic configurations.[1] As a result of the large energy gaps between their ground and first excited states which limit non-radiative relaxation, Eu^{III} and Tb^{III} have been used for the development of luminescent structural probes in biological materials[2] and long-lived emitting stains for homogeneous fluoroimmunoassays.[3] Recently, many authors have taken advantage of the large magnetic moment and the slow electronic relaxation rate of gadolinium(III) complexes for the preparation of contrast agents in NMR imaging.[4] However, the design of lanthanide complexes with predetermined physicochemical properties requires a strict structural and topological control of the co-ordination sphere around the metal ion,[1,5] and this represents a synthetic challenge since Ln^{III} display large and variable co-ordination numbers with little stereochemical preferences.[6] According to the lock-and-key principle,[7] most of the specific molecular receptors developed so far for the selective and structurally controlled complexation of Ln^{III} have cyclic,[8] bicyclic[9,10] or podand[9,11] structures to main-

tain the binding units in an appropriate orientation for them efficiently to co-ordinate the metal. Nonetheless, the fine tuning of the structural and electronic properties of the receptors is severely limited by the tedious syntheses of rigid macro-polycyclic compounds.[12] Inspired by the induced fit concept[13] and the formation of stable mononuclear helical complexes [LnL$^1_3$]$^{3+}$ (L^1 = 2,2′:6′,2″-terpyridine) with the complete lanthanide series,[14] we have suggested that weak secondary non-covalent interactions associated with complexation processes might contribute to the selective introduction of Ln^{III} into organized edifices.[15] We have found that the analogous compound L^2 displays a pronounced preference for the lighter lanthanide(III) ions (La–Ho) as a result of intramolecular π-stacking interactions between the ligand strands which prevent the contraction of the co-ordination cavity required for the complexation of the smallest ions (Er–Lu).[15,16] An improved structural control of the final architecture may be obtained by the use of 3d-block tripods in self-assembled triple-stranded heterodinuclear d–f complexes [LnML$^3_3$]$^{5+}$ (Ln = La–Lu, M = Fe or Zn).[17,18] In these complexes, the 3d ion is co-ordinated by the three bidentate units of the segmental ligand L^3 in a facial pseudo-octahedral arrangement producing a non-covalent tri-podal spacer which organizes the three remaining tridentate binding units for their pseudo-tricapped trigonal-prismatic (ttp) co-ordination around Ln^{III}. However, the low stability and the faint luminescence of [EuZnL$^3_3$]$^{5+}$ associated with the closely packed arrangement of the ligands[16] prompted us to replace the terminal benzimidazole group of L^3 with an *N,N*-diethylcarboxamide group in L^4, leading to the strongly lumi-

L^1

L^2

L^3

L^4

L^5

L^6

$[EuZnL^4_3]^{5+}$

nescent and water-resistant non-covalent podate $[EuZnL^4_3]^{5+}$.[19] Detailed thermodynamic, structural and photophysical studies show that the 3d ion (*i*) plays a crucial role in the assembly process and (*ii*) finely controls the arrangement of the ligand strands around Ln^{III}.[20] Moreover, a synergetic effect is expected and the introduction of different lanthanide ions into the heterodinuclear edifices might exert some structural and electronic control over the 3d-block co-ordination site. Iron(II) is particularly suitable as a structural and spectroscopic probe since its spin state, spectroscopic and magnetic properties are very sensitive to its co-ordination environment.[21] When Fe^{II} is pseudo-octahedrally co-ordinated by three bidentate α,α'-diimine units as expected in $[LnFeL^4_3]^{5+}$ an equilibrium between diamagnetic low-spin ($^1A_1$) and paramagnetic high-spin ($^5T_2$) states is often observed.[18,22] This spin transition is related to molecular bistability[23] and may lead to the development of active elements for memory devices if the following requirements are fulfilled: (*i*) the spin transition is abrupt and occurs with a large hysteresis, (*ii*) the transition temperature must be close to room temperature and (*iii*) an easily detectable response is associated with the transition.[24] Point (*i*) is closely related to co-operativity resulting from strong intermolecular interactions and is hard to design, but (*ii*) and (*iii*) could be addressed by the choice of suitable lanthanide ions in the heterodinuclear d–f podates.

In this paper we report the synthesis and characterization of the self-assembled and magnetically active triple-stranded non-covalent lanthanide podates $[LnFeL^4_3]^{5+}$ (Ln = La–Lu). Particular attention is focused on the influence of the structurally demanding Fe^{II} on the lanthanide co-ordination site together with the synergetic control exerted by Ln^{III} on the enthalpic and entropic parameters of the iron(II) spin transition.
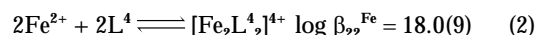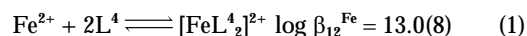
Results and Discussion

The ligand L^4 possesses two different binding units coded for the simultaneous recognition of 3d and 4f ions,[19,20] and the formation of the planned heterodinuclear triple-stranded helical non-covalent podates $[LnFeL^4_3]^{5+}$ implies an elaborate assembly process involving three different components: Ln^{III},

Fe^{II} and L^4.[25] Our strategy is thus based on the following approach: (*i*) study of the homopolynuclear complexes formed by L^4 with La^{III} and Fe^{II} and (*ii*) complete characterization of the assembly process using electrospray mass spectrometry for qualitative speciation[26] and spectrophotometric titrations for the quantitative estimation of the thermodynamic equilibria.[20,27] This allows the determination of a reliable set of conditions for which the heterodinuclear complexes $[LnFeL^4_3]^{5+}$ are quantitatively formed in solution and can be then structurally characterized using spectroscopic and magnetic techniques.[20]

Homonuclear complexes of L^4 with La^{III} and Fe^{II}

Compound L^4 was shown to react with $La(ClO_4)_3$ to give a mixture of at least four complexes $[LaL^4_3]^{3+}$, $[La_2L^4_3]^{6+}$, $[La_2L^4_2]^{6+}$ and $[La_3L^4_2]^{9+}$ in acetonitrile as a result of the poor matching between the binding possibilities of the ligand and the stereochemical requirements of Ln^{III}.[20] Electrospray mass spectrometric titrations of L^4 (0.2 mmol dm^{-3}) by $Fe(ClO_4)_2$ in acetonitrile for $Fe^{II}:L^4$ ratios in the range 0.3–1.5:1 evidence a mixture of $[FeL^4_3]^{2+}$, $[FeL^4_2]^{2+}$, $[Fe_2L^4_3]^{4+}$, $[FeL^4]^{2+}$ and $[Fe_2L^4_2]^{4+}$. The last two complexes display the same m/z ratio, but possess different isotopic patterns and adduct ions with perchlorate which allow their unambiguous characterization (Table 1).[26,27] Spectrophotometric titrations under the same conditions result in complicated variations of the spectra with a final end-point for an $Fe:L^4$ ratio of 1:2. Factor analysis[28] suggests that only three absorbing species are necessary to reproduce the experimental data which can thus be satisfactorily fitted by equilibria (1) and (2) using non-linear least-squares

$$Fe^{2+} + 2L^4 \rightleftharpoons [FeL^4_2]^{2+} \quad \log \beta_{12}^{Fe} = 13.0(8) \quad (1)$$

$$2Fe^{2+} + 2L^4 \rightleftharpoons [Fe_2L^4_2]^{4+} \quad \log \beta_{22}^{Fe} = 18.0(9) \quad (2)$$

methods[29] (root-mean-square difference between calculated and observed absorbances, 0.004). Attempts to include supplementary absorbing complexes such as $[FeL^4_3]^{2+}$ and $[Fe_2L^4_3]^{4+}$ in the fitting process failed as a result of the great similarity between the reconstituted spectra.

Table 1 Molecular peaks of complexes of L^4 and adduct ions observed by electrospray mass spectrometry

| Metal	Cation	m/z^*
Fe^{II}	$[FeL^4_3]^{2+}$	843.4
	$[FeL^4_3(ClO_4)]^+$	1785.8
	$[FeL^4_2]^{2+}$	571.2
	$[FeL^4_2(ClO_4)]^+$	1241.4
	$[Fe_2L^4_3]^{4+}$	435.6
	$[Fe_2L^4_3(ClO_4)]^{3+}$	614.0
	$[Fe_2L^4_3(ClO_4)_2]^{2+}$	970.4
	$[Fe_2L^4_2]^{4+}$	299.6
	$[Fe_2L^4_2(ClO_4)]^{3+}$	432.0
	$[Fe_2L^4_2(ClO_4)_2]^{2+}$	698.2
	$[FeL^4]^{2+}$	299.6
	$[FeL^4(ClO_4)]^+$	698.2
La^{III}/Fe^{II}	$[LaFeL^4_3]^{5+}$	365.1
	$[LaFeL^4_3(ClO_4)]^{4+}$	481.3
	$[LaFeL^4_3(ClO_4)_2]^{3+}$	674.9
	$[LaFeL^4_3(ClO_4)_3]^{2+}$	1062.1
	$[FeL^4_2]^{2+}$	571.3
Eu^{III}/Fe^{II}	$[EuFeL^4_3]^{5+}$	367.5
	$[EuFeL^4_3(ClO_4)]^{4+}$	484.6
	$[EuFeL^4_3(ClO_4)_2]^{3+}$	679.0
	$[EuFeL^4_3(ClO_4)_3]^{2+}$	1068.9
	$[FeL^4_2]^{2+}$	571.6
Gd^{III}/Fe^{II}	$[GdFeL^4_3]^{5+}$	368.6
	$[GdFeL^4_3(ClO_4)]^{4+}$	485.6
	$[GdFeL^4_3(ClO_4)]^{4+}$	681.2
	$[GdFeL^4_3(ClO_4)_3]^{2+}$	1071.4
	$[FeL^4_2]^{2+}$	571.2
Tb^{III}/Fe^{II}	$[TbFeL^4_3]^{5+}$	368.9
	$[TbFeL^4_3(ClO_4)]^{4+}$	486.2
	$[TbFeL^4_3(ClO_4)_2]^{3+}$	681.6
	$[TbFeL^4_3(ClO_4)_3]^{2+}$	1072.4
	$[FeL^4_2]^{2+}$	571.2
Lu^{III}/Fe^{II}	$[LuFeL^4_3]^{5+}$	372.2
	$[LuFeL^4_3(ClO_4)]^{4+}$	490.0
	$[LuFeL^4_3(ClO_4)_2]^{3+}$	686.8
	$[LuFeL^4_3(ClO_4)_3]^{2+}$	1079.8
	$[FeL^4_2]^{2+}$	571.2

* m/z values given for the maximum of the peak.

The stability constants proposed for equilibria (1) and (2) are thus only rough estimations and do not reflect accurately the complicated thermodynamic equilibria occurring in solution. This behaviour sharply contrasts with the formation of only two well defined complexes $[FeL^3_2]^{2+}$ [log $\beta_{12}^{Fe} = 14.1(4)$] and $[Fe_2L^3_2]^{4+}$ [log $\beta_{22}^{Fe} = 20.0(8)$] with the analogous ligand L^3.[18] The replacement of the terminal benzimidazole group of L^3 by a carboxamide group in L^4 significantly affects the complexation properties of the tridentate units for soft 3d ions. Pseudo-octahedral co-ordination of the tridentate units to Fe^{II} becomes less favourable and leads to mixtures of complexes with variable stoichiometries as similarly observed with Zn^{II}.[17,20] Proton NMR titrations of L^4 by $Fe(ClO_4)_2$ in CD_3CN confirm the spectrophotometric results and show poorly resolved paramagnetic signals for $Fe:L^4$ ratios in the range $0.1–0.9:1$. For $Fe:L^4 = 1.0$ the spectrum is sharply resolved, displays 20 bands spread over 80 ppm and is compatible with a C_s-symmetrical mononuclear complex $[FeL^4]^{2+}$ or a C_2-symmetrical dinuclear species $[Fe_2L^4_2]^{4+}$ analogous to the head-to-tail double-stranded helicate $[Zn_2L^4_2]^{4+}$.[20] However, the increased relaxation rate induced by the paramagnetic Fe^{II} prevents reliable correlation (COSY) or nuclear Overhauser effect (NOESY) spectra to be recorded and the structure of this complex was not further investigated.

Self-assembly of heterodinuclear complexes $[LnFeL^4_3]^{5+}$

The addition of an equimolar mixture of $Fe(ClO_4)_2$ and $Ln(ClO_4)_3$ (Ln = La, Eu, Gd, Tb or Lu) to a solution of L^4 (5×10^{-4} mol dm^{-3}) greatly simplifies the electrospray mass

spectrometric titration and peaks corresponding to only two different complexes $[FeL^4_2]^{2+}$ and $[LnFeL^4_3]^{5+}$ are observed together with those of the ligand $[L^4 + H]^+$ (m/z 544.3) and $[L^4 + 2H]^{2+}$ (m/z 272.7) (Fig. 1). At lower concentration ($[L^4]_t = 5 \times 10^{-5}$ mol dm^{-3}), $[FeL^4_2]^{2+}$ and $[LnFeL^4_3]^{5+}$ are still the major species in solution, but a small peak attributed to $[FeL^4_3]^{2+}$ becomes significant. For $[L^4]_t = 5 \times 10^{-6}$ mol dm^{-3} the free pro-ligand only is detected [Fig. 1(c)]. Spectrophotometric titrations of L^4 (0.5 mmol dm^{-3}) by equimolar mixtures of $Fe(ClO_4)_2$ and $Ln(ClO_4)_3$ (Ln = La, Eu or Lu) confirm these results and display a monotonous evolution of the absorbances with an end-point for $M:L^4 = 0.35:1$ (M = $[Ln^{III}] = [Fe^{II}]$, Fig. 2). Factor analysis[28] reveals three absorbing species and the data were fitted by equilibria (1) and (3) yielding log

$$Ln^{3+} + Fe^{2+} + 3L^4 \xrightleftharpoons{\log \beta_{113}^{LnFe}} [LnFeL^4_3]^{5+} \qquad (3)$$
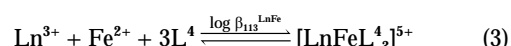
$\beta_{12}^{Fe} = 13.5(8)$, log $\beta_{113}^{LaFe} = 23.0(8)$, log $\beta_{113}^{EuFe} = 24.6(9)$ and log $\beta_{113}^{LuFe} = 23.6(7)$.

This approach is oversimplified since at least nine equilibria [eight involving homonuclear complexes and (3)] should be considered, but the differences between the spectra of the complexes are insufficient to allow an accurate mathematical treatment.[30] However, the same experimental conditions are used for electrospray mass spectrometric and for spectrophotometric titrations and Lehn and co-workers[27] have recently proposed that the strict consideration of the species observed by electrospray in solution for d-block supramolecular complexes provides a minimum set of intermediates, which facilitates the analysis of spectrophotometric titration curves in multi-component assemblies and gives satisfying results. Although this simplified model leads to mere estimations of the stability constants, the values of log β_{12}^{Fe} extracted from the titration of L^4 by an equimolar mixture of Fe^{II} and Ln^{III} (Ln = La, Eu or Lu) are consistent with those found from the direct titration and the distribution curves [Fig. 2(b) and 2(c)] calculated from equations (1) and (3) are in good qualitative agreement with the mass spectrometric results (significant formation of $[FeL^4_2]^{2+}$ for $[L^4]_t = ca.$ 10^{-4} mol dm^{-3}) and the NMR data (quantitative formation of $[LnFeL^4_3]^{5+}$ for $[L^4]_t > 10^{-2}$ mol dm^{-3} and $Ln^{III}:Fe^{II}:L^4 = 1:1:3$; see below). The estimated stability constants log β_{113}^{LnFe} are significantly smaller than those reported for the analogous $[LnZnL^4_3]^{5+}$ podates [log $\beta_{113}^{LaZn} = 29.0(4)$ and log $\beta_{113}^{EuZn} = 28.6(6)$],[20] which suggests that the stereochemically demanding Fe^{II} decreases the stability of the heterodinuclear complexes.

Solution structure of $[LnFeL^4_3]^{5+}$

Absorption spectral data for 1.12×10^{-3} mol dm^{-3} $[LnFeL^4_3]^{5+}$ (Ln = La, Nd, Eu, Gd, Tb, Yb, Lu or Y) in acetonitrile, a concentration at which the $[LnFeL^4_3]^{5+}$ species is formed at 96%, are reported in Table 2. They are dominated by broad and intense ligand-centred $\pi \longrightarrow \pi^*$ transitions around 30 000 cm^{-1} displaying a shoulder to low energy, which is typical of the co-ordination of both bi- and tri-dentate binding units[16–19] as discussed for the analogous LnZn podates.[20] A large and poorly structured m.l.c.t. (metal-to-ligand charge transfer) transition ($Fe^{II} \longrightarrow \pi^*$) occurring in the range 19 010–19 080 cm^{-1} is responsible for the deep red colour of the complexes in solution as similarly found for $[Fe(bipy)_3]^{2+}$ (bipy = 2,2′-bipyridine; 19 160 cm^{-1}),[31] $[LnFeL^3_3]^{5+}$ (Ln = La–Eu; 19 000 cm^{-1})[20] and $[FeL^5_3]^{2+}$ (19 230 cm^{-1})[32] where Fe^{II} is pseudo-octahedrally co-ordinated by three α,α'-diimine ligands. We conclude that Fe^{II} also occupies a pseudo-octahedral co-ordination site provided by the three bidentate binding units of L^4 which adopt the expected head-to-head arrangement in $[LnFeL^4_3]^{5+}$, as found in $[LnZnL^4_3]^{5+}$.[18–20] The m.l.c.t. band displays a pronounced thermochromic behaviour between 233 and 333 K for all the
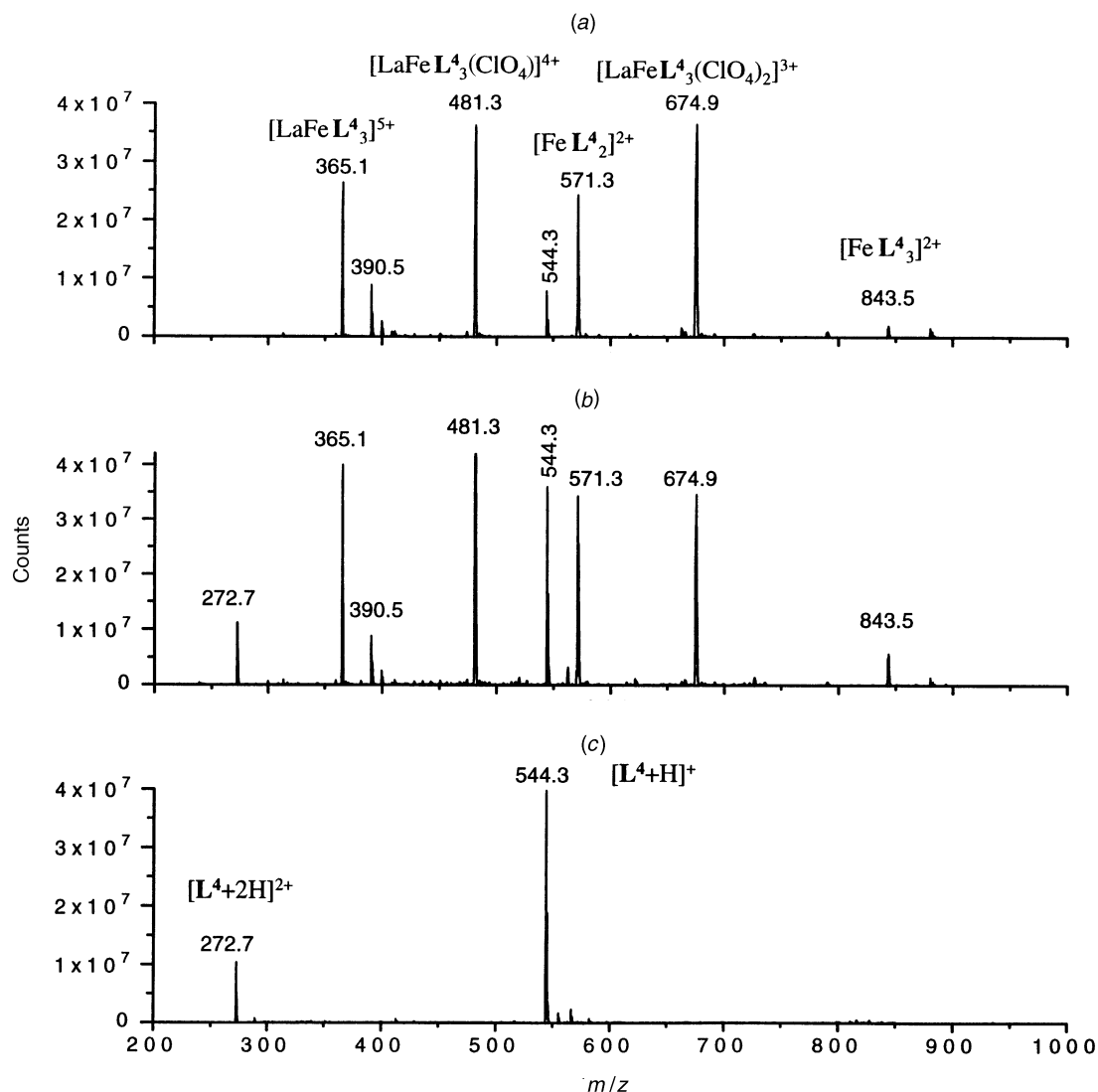
Fig. 1 Electrospray mass spectra of $[LaFeL^4_3]^{5+}$ in acetonitrile for total ligand concentrations of (*a*) 5×10^{-4}, (*b*) 5×10^{-5} and (*c*) 5×10^{-6} mol dm^{-3}

Ln^{III} studied (Fig. 3) pointing to an iron(II) spin-state equilibrium similar to those found for $[FeL^5_3]^{2+}$ [32] and $[LnFeL^4_3]^{5+}$ (Ln = La–Eu).[18] The significant decrease of the molar absorbance of the m.l.c.t. band at high temperature corresponds to depopulation of the $^1A_1$ low-spin state which is responsible for the intense m.l.c.t. transition [22,31] since $^5T_2$ high-spin Fe^{II} is expected to give much weaker charge-transfer bands.[22,33] A quantitative analysis of this partial spin-crossover behaviour is described below. The ligand-field strength around Fe^{II} could not be determined because the d–d transitions are obscured by the intense m.l.c.t. band.

The location of Fe^{II} in a pseudo-octahedral site is confirmed by cyclic voltammograms in acetonitrile which show $[LnFeL^4_3]^{5+}$ (Ln = La, Nd, Eu, Yb, Lu or Y) to be oxidized in a reversible one-electron wave at $E_\frac{1}{2} = 0.82$ V *vs.* saturated calomel electrode (SCE) (Fe^{III}–Fe^{II}, $E_p^a - E_p^c = 65–85$ mV, Table 2) as similarly reported for $[Fe(bipy)_3]^{2+}$ ($E_\frac{1}{2} = 0.79$ V)[34] and $[LnFeL^3_3]^{5+}$ (Ln = La–Eu, $E_\frac{1}{2} = 0.82–0.84$ V).[18] No significant variation of the potentials of the Fe^{III}–Fe^{II} couple is observed for the different Ln^{III}, but the reduction of the complexes depends on the Ln^{III} studied. For Ln = La, Nd or Y which cannot be reduced easily[35] we observe three successive cathodic waves tentatively attributed to ligand-centred reductions as described for $[Fe(bipy)_3]^{2+}$.[18,36] For $[EuFeL^4_3]^{5+}$, a supplementary quasi-reversible wave is observed at $E_\frac{1}{2} = -0.58$ V *vs.* SCE (Eu^{II}–Eu^{II}, $E_p^a - E_p^c = 100$ mV) which is ascribed to the reduction of Eu^{III} to Eu^{II}. Compared to the reduction potential of

solvated Eu^{3+} in MeCN ($E_\frac{1}{2} = 0.21$ V *vs.* SCE),[37] the reduction of Eu^{III} in $[EuFeL^4_3]^{5+}$ is significantly shifted toward negative values despite the higher charge of the complex. This may arise from the co-ordination of the carboxamide groups of ligand L^4 to Eu^{III} which are known to destabilize Eu^{II} as observed in dimethylformamide ($E_\frac{1}{2} = -0.71$ V *vs.* SCE) and in dimethylacetamide ($E_\frac{1}{2} = -0.60$ V *vs.* SCE).[37] Europium(III) thus occupies the pseudo-ttp site produced by the three wrapped tridentate L^4.[20] Taking into account the Eu^{III}–Eu^{II} potentials of solvated and complexed Eu^{III} in MeCN, we can estimate the ratio of the stability constants,[38] log $(\beta_{113}^{Eu^{II}Fe}/\beta_{113}^{Eu^{III}Fe}) = \{E_\frac{1}{2}([EuFeL^4_3]^{5+}) - E_\frac{1}{2}(Eu^{3+})\}/0.059 = -13.4$, a value significantly more negative than that found for the mononuclear complex $[EuL^2_3]^{3+}$ (-7.8)[39] where Eu is co-ordinated by nine heterocyclic nitrogen-donor atoms. Since the stability constants of $[EuL^2_3]^{3+}$ and $[EuL^6_3]^{3+}$ are similar in acetonitrile,[39] we conclude that the carboxamide groups of the tridentate unit destabilize the europium(II) complexes. The reduction of Yb^{III} in $[YbFeL^4_3]^{5+}$ is expected at significantly more negative values[37] and is observed at -1.46 V *vs.* SCE as a poorly resolved wave obscured by the ligand-centred reductions.

The solution structure of $[LnFeL^4_3]^{5+}$ (Ln = La, Nd, Eu, Yb, Lu, Y or Sc) and $[CaFeL^4_3]^{4+}$ has been unambiguously established by ^1H NMR spectroscopy (Table 3). The spectra display 23 signals corresponding to three equivalent non-planar strands related by a C_3 axis ($H^{7,8}$, $H^{15,16}$ and $H^{17,18}$ are diastereotopic).[40] The short electronic relaxation time of the Ln^{III} studied pro-

Table 2 Electronic spectral data for L^4 and $[LnFeL^4_3]^{5+}$ in MeCN [a] and electrochemical reduction potentials in MeCN + 0.1 mol dm^{-3} NBu$_4$PF$_6$ [b] at 293 K

Compound	$\pi \longrightarrow \pi^*$	m.l.c.t.	$E_{\frac{1}{2}}$	$E_p^a - E_p^c$
L^4	33 320 (50 690)			
	31 750 (39 090) (sh)			
$[LaFeL^4_3]^{5+}$	29 940 (116 890)	24 750 (2560) (sh)	+ 0.82 [c]	65
	28 570 (86 790) (sh)	19 800 (4590) (sh)	− 1.25 [d]	65
		19 050 (4660)	− 1.42 [d]	120
			− 1.60 [d]	Irreversible
$[NdFeL^4_3]^{5+}$	30 030 (116 630)	24 750 (2780) (sh)	+ 0.82 [c]	65
	28 570 (85 810) (sh)	19 800 (4950) (sh)	− 1.12 [d]	65
		19 050 (5044)	− 1.38 [d]	70
			− 1.43 [d]	120
$[EuFeL^4_3]^{5+}$	29 940 (118 760)	24 750 (2860) (sh)	+ 0.82 [c]	70
	28 570 (92 700) (sh)	19 800 (4970) (sh)	− 0.58 [e]	100
		19 010 (5050)	− 1.42 [d]	85
			− 1.68 [d]	Irreversible
$[GdFeL^4_3]^{5+}$	29 940 (117 680)	24 750 (2740) (sh)		
	28 570 (90 500) (sh)	19 800 (4940) (sh)		
		19 050 (5000)		
$[TbFeL^4_3]^{5+}$	29 850 (118 130)	24 750 (2740) (sh)		
	28 570 (91 800) (sh)	19 800 (4940) (sh)		
		19 080 (5000)		
$[YbFeL^4_3]^{5+}$	29 940 (116 890)	24 750 (2690) (sh)	+ 0.82 [c]	85
	28 570 (89 740) (sh)	19 800 (4700) (sh)	− 1.12 [d]	80
		19 010 (4800)	− 1.37 [d]	90
			− 1.46 [d,e]	90
$[LuFeL^4_3]^{5+}$	29 940 (118 110)	24 750 (2730) (sh)	+ 0.82 [c]	70
	28 570 (89 920) (sh)	19 800 (4980) (sh)	− 1.15 [d]	65
		19 080 (5100)	− 1.42 [d]	140
			− 1.57 [d]	Irreversible
$[YFeL^4_3]^{5+}$	29 850 (118 940)	24 750 (2640) (sh)	+ 0.82 [c]	65
	28 570 (89 980) (sh)	19 800 (4650) (sh)	− 1.17 [d]	65
		19 080 (4750)	− 1.41 [d]	110
			− 1.67 [d]	Irreversible

[a] Energies are given for the maximum of the band envelope in cm^{-1} and ε (in parentheses) in dm^3 mol^{-1} cm^{-1}; sh = shoulder. [b] Electrochemical potentials are given in V *vs.* SCE and $(E_p^a - E_p^c)$ in mV. Estimated error on $E_{\frac{1}{2}}$ is ± 0.01 V. [c] Oxidation of Fe^{II}. [d] Reduction centred on the ligand. [e] Reduction centred on Ln^{III}.
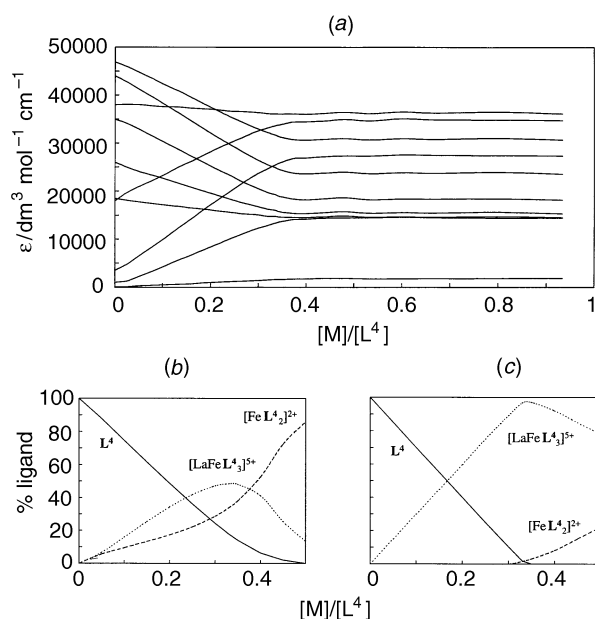

Fig. 2 (*a*) Variation of the observed molar absorption coefficient at 10 different wavelengths for the spectrophotometric titration of L^4 with an equimolar mixture of Fe(ClO$_4$)$_2$·6H$_2$O and La(ClO$_4$)$_3$·6H$_2$O ([M] = [Ln^{III}] = [Fe^{II}]; total ligand concentration = 10^{-4} mol dm^{-3}) in MeCN at 293 K and corresponding calculated speciation of the ligand for total ligand concentrations of (*b*) 10^{-4} and (*c*) 10^{-2} mol dm^{-3}

Fig. 3 Visible spectra of $[LaFeL^4_3]^{5+}$ in MeCN at stepwise decreasing temperature (ΔT = 10 K) between (*a*) 333 and (*i*) 243 K and calculated visible spectra for pure high-spin (· · ·) and low-spin (– – –) $[LaFeL^4_3]^{5+}$. Complex concentration: 1.2 mmol dm^{-3}

duce little line broadening [41] allowing reliable nuclear Overhauser effects (NOEs) and two-dimensional-COSY correlation spectra to be detected. Intra- and inter-strand NOEs are char-
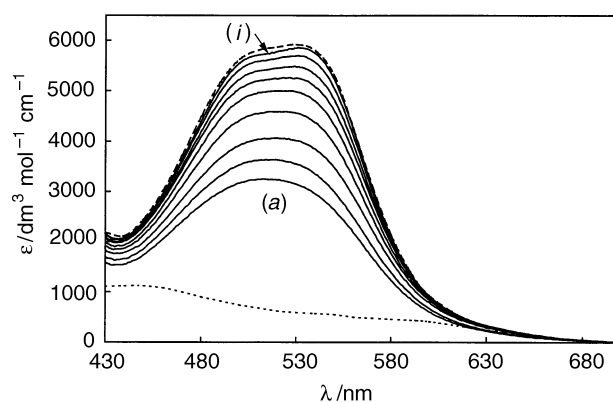
acteristic of the helical twist and close packing of the strands previously described for $[LnFeL^3_3]^{5+}$ [18] and $[LnZnL^4_3]^{5+}$. [20] The complexes $[LnFeL^4_3]^{5+}$ thus adopt a C_3-symmetrical head-to-head triple-helical structure very similar to that established for the analogous LnZn podates. [19,20] For a given Ln^{III}, the chemical shifts of the protons of the tridentate binding unit in $[LnFeL^4_3]^{5+}$ are similar to those found for $[LnZnL^4_3]^{5+}$ which indicates that Ln^{III} occupies the same pseudo-ttp co-ordination site. However, the ^{1}H NMR signals of the protons of the bidentate units are completely different for $[LnFeL^4_3]^{5+}$ compared to $[LnZnL^4_3]^{5+}$ even for the diamagnetic Ln^{III}. [20] When going from $[LaZnL^4_3]^{5+}$ to $[LaFeL^4_3]^{5+}$, H^2 and H^6 are shielded by

Table 3 Proton NMR shifts (with respect to SiMe$_4$) of [LnFeL$^4_3$]$^{5+}$ in CD$_3$CN at 298 K

Bidentate binding unit

Compound	Me^1	Me^2	H^1	H^2	H^3	H^4	H^5	H^6	H^{7,8}
[LaZnL$^4_3$]$^{5+}$	2.15	4.21	7.74	7.84	8.17	7.61	7.22	5.42	3.53,3.64
[LaFeL$^4_3$]$^{5+}$ *	2.05	4.61	8.30	7.68	9.30	7.98	7.00	4.14	3.39,3.59
[LaFeL$^4_3$]$^{5+}$	1.97	7.08	20.2	6.76	18.4	11.59	6.81	2.74	3.28,3.61
[YFeL$^4_3$]$^{5+}$	1.98	6.68	18.3	6.91	17.0	11.04	6.88	2.88	3.29,3.59
[LuFeL$^4_3$]$^{5+}$	1.98	6.48	17.4	7.00	16.2	10.75	6.89	2.94	3.29,3.59
[NdFeL$^4_3$]$^{5+}$	1.79	6.66	19.4	6.57	17.8	11.14	6.59	1.30	2.93,3.15
[EuFeL$^4_3$]$^{5+}$	2.19	7.22	19.8	7.07	18.0	11.74	7.20	4.60	3.74,4.12
[YbFeL$^4_3$]$^{5+}$	2.40	7.25	18.8	7.43	17.15	11.72	7.72	6.39	3.86,4.53
[ScFeL$^4_3$]$^{5+}$	1.97	6.07	15.2	7.15	14.7	10.12	6.90	3.14	3.37,3.57
[CaFeL$^4_3$]$^{4+}$	1.98	6.91	19.5	6.78	17.8	11.30	6.79	2.85	3.20,3.56

Tridentate binding unit

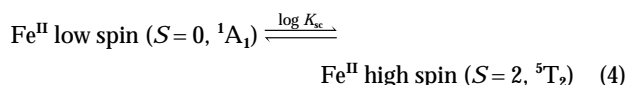| Compound	Me^3	H^9	H^{10}	H^{11}	H^{12}	H^{13}	H^{14}	H^{15,16}	H^{17,18}	Me^4	Me^5
[LaZnL$^4_3$]$^{5+}$	4.33	5.82	6.96	7.35	8.52	8.35	7.82	2.84	3.34 3.42	0.75	0.92
[LaFeL$^4_3$]$^{5+}$ *	4.35	5.60	6.99	7.57	8.50	8.28	7.74	2.78	3.30 3.32	0.65	0.96
[LaFeL$^4_3$]$^{5+}$	4.23	4.83	6.93	7.41	8.36	8.20	7.65	2.71	3.19 3.28	0.62	0.81
[YFeL$^4_3$]$^{5+}$	4.27	4.56	6.88	7.37	8.43	8.18	7.69	2.54 2.67	3.27 3.32	0.58	0.92
[LuFeL$^4_3$]$^{5+}$	4.28	4.52	6.91	7.39	8.46	8.18	7.70	2.50 2.66	3.28 3.35	0.52	0.96
[NdFeL$^4_3$]$^{5+}$	4.94	0.45	6.60	8.11	11.05	9.73	9.24	2.48 3.00	3.58 3.96	−1.01	1.29
[YbFeL$^4_3$]$^{5+}$	2.56	14.93	7.45	7.01	4.70	5.90	5.98	1.63 2.61	1.82 3.24	4.63	−0.21
[ScFeL$^4_3$]$^{5+}$	4.29	4.48	6.92	7.38	8.44	8.12	7.70	2.42 2.68	3.36 3.36	0.56	1.03
[CaFeL$^4_3$]$^{4+}$	4.15	4.84	6.77	7.24	8.10	7.92	7.35	2.45 2.63	2.80 3.05	0.49	0.60

* At 233 K.

$\Delta\delta = -1.08$ and -2.68 ppm respectively) while H^1, H^3 and H^4 are strongly shifted toward lower field ($\Delta\delta = 12.46$, 10.23 and 3.98 ppm respectively) as a result of the spin-state equilibrium in [LaFeL$^4_3$]$^{5+}$ at room temperature, as reported for analogous [LaFeL$^3_3$]$^{5+}$.[18] Short longitudinal relaxation times for the protons of the bidentate units of [LaFeL$^4_3$]$^{5+}$ at 298 K (SUP 57202) result from the coupling between the ^{1}H nuclear magnetic moments and the magnetic moment of high-spin Fe^{II},[42] while decreasing the temperature to 233 K restores an essentially diamagnetic ^{1}H NMR spectrum for [LaFeL$^4_3$]$^{5+}$ comparable to that found for [LaZnL$^4_3$]$^{5+}$,[20] which confirms the existence of a thermally induced spin-crossover behaviour for [LaFeL$^4_3$]$^{5+}$ (Fig. 4). Detailed investigations of the ^{1}H NMR spectra of [LnFeL$^4_3$]$^{5+}$ (Ln = La, Nd, Eu, Yb, Lu or Y) in the temperature range 233–333 K, at various concentrations (0.3–1.0 mol dm^{-3}) and upon addition of an excess of pro-ligand, show that (*i*) the C_3-symmetrical triple-helical complexes [LnFeL$^4_3$]$^{5+}$ are the only ones observed in solution, (*ii*) the ligand-exchange processes are slow on the NMR time-scale as judged from the well resolved NMR signals observed for the free pro-ligand when an excess of L^4 is added to a solution of the complex and (*iii*) the spin-state equilibrium is fast on the NMR time-scale.[43] For [ScFeL$^4_3$]$^{5+}$ the triple-helical complex is the only complex in solution between 273 and 333 K. Below 273 K some poorly resolved signals corresponding to those observed for mixtures of [FeL$^4_3$]$^{2+}$, [FeL$^4_2$]$^{2+}$ and [Fe$_2$L$^4_4$]$^{4+}$ appear together with the heterodinuclear complex suggesting that some decomplexation occurs. This correlation between the size of the metal ion in the ttp co-ordination site and the stability of the complex is confirmed for Ca^{II} which gives selectively and quantitatively [CaFeL$^4_3$]$^{4+}$ in solution, the ^{1}H NMR spectrum of which displays chemical shifts very similar to those observed for

[LaFeL$^4_3$]$^{5+}$ which indicates that the charge of the metal ion in the pseudo-ttp site is not crucial for the formation of the triple-helical podate. Attempts to introduce Al^{III} into the heterodinuclear complexes failed and intricate mixtures of homo- and hetero-dinuclear complexes were observed even after thermodynamic equilibration of the inert aluminium(III) complexes. This observation, together with the reduced stability of [ScFeL$^4_3$]$^{5+}$, suggests that only sufficiently large spherical metal ions such as Ln^{III} [44] are suitable to self-assemble with Fe^{II} and L^4 to give heterodinuclear complexes in quantitative yield.

Iron(II) spin-state equilibria of [MFeL$^4_3$]$^{5+}$ (M = La, Nd, Eu, Yb, Lu, Y or Sc) and [CaFeL$^4_3$]$^{4+}$ in acetonitrile

The pronounced thermochromism of [LnFeL$^4_3$]$^{5+}$ and the temperature-dependent ^{1}H NMR spectra are typical of spin-state equilibria (4). Magnetic moments μ_{eff} (Table 4) have been

$$\text{Fe}^{II} \text{ low spin } (S = 0, \, ^1\text{A}_1) \xrightarrow{\log K_{sc}}$$
$$\text{Fe}^{II} \text{ high spin } (S = 2, \, ^5\text{T}_2) \quad (4)$$

determined according to the Evans method[45–48] and using the diamagnetic-correction procedure described by one of us for supramolecular complexes.[49] For the heteronuclear complexes [MFeL$^4_3$]$^{5+}$ with diamagnetic ions (M = La, Lu, Y or Sc) and [CaFeL$^4_3$]$^{4+}$ the measured magnetic moments directly reflect the electronic structure of Fe^{II}. We observe a smooth and monotonous increase of μ_{eff} from 0.5–0.6 μ_B at 233 K to 3.1–3.5 μ_B at 333 K which fall between the pure low-spin ($\mu_{eff} = 0$–0.5 μ_B) and the pure high-spin limits ($\mu_{eff} = 5.0$–5.5 μ_B) typically found for other iron(II) complexes.[18,22,32,43] Assuming that no inter-

Table 4 Effective total magnetic moments μ_{eff}/μ_B,[a] effective magnetic moments of Fe^{II}, $\mu_{eff}(Fe)/\mu_B$,[b] and calculated mole fractions of high-spin Fe^{II} (x_{hs}) for $[LnFeL^4_3][ClO_4]_5$, $[CaFeL^4_3][ClO_4]_4$ and $[LnZnL^4_3][ClO_4]_5$ at different temperatures in acetonitrile

		T/K										
		233	243	253	263	273	283	293	303	313	323	333
LaFe	μ_{eff}	0.58	0.78	0.99	1.25	1.51	1.82	2.25	2.54	2.91	3.25	3.56
	x_{hs}	0.01	0.02	0.03	0.05	0.09	0.13	0.19	0.26	0.34	0.43	0.51
LuFe	μ_{eff}	0.57	0.71	0.93	1.14	1.35	1.62	1.85	2.18	2.50	2.86	3.20
	x_{hs}	0.01	0.01	0.03	0.04	0.07	0.10	0.14	0.20	0.26	0.33	0.41
YFe	μ_{eff}	0.57	0.76	0.94	1.17	1.41	1.71	2.09	2.38	2.72	3.07	3.40
	x_{hs}	0.01	0.02	0.03	0.05	0.08	0.12	0.17	0.23	0.30	0.38	0.48
ScFe	μ_{eff}	0.95	1.09	1.21	1.36	1.54	1.74	1.95	2.25	2.53	2.84	3.11
	x_{hs}	0.01	0.02	0.03	0.05	0.08	0.11	0.16	0.21	0.27	0.33	0.40
CaFe	μ_{eff}	0.58	0.71	0.93	1.17	1.41	1.72	2.07	2.41	2.77	3.12	3.46
	x_{hs}	0.01	0.02	0.03	0.05	0.08	0.12	0.17	0.24	0.31	0.39	0.48
NdZn	μ_{eff}	3.35	3.54	3.54	3.55	3.56	3.57	3.58	3.58	3.59	3.58	3.57
NdFe	μ_{eff}	3.59	3.63	3.69	3.77	3.87	4.01	4.18	4.36	4.57	4.79	5.00
	$\mu_{eff}(Fe)$	0.59	0.73	0.98	1.20	1.49	1.78	2.13	2.47	2.82	3.17	3.49
	x_{hs}	0.01	0.02	0.03	0.05	0.08	0.12	0.18	0.25	0.33	0.41	0.49
EuZn	μ_{eff}	3.21	3.24	3.28	3.31	3.35	3.38	3.41	3.44	3.46	3.48	3.52
EuFe	μ_{eff}	3.47	3.54	3.63	3.73	3.84	3.99	4.18	4.36	4.58	4.82	5.05
	$\mu_{eff}(Fe)$	0.58	0.79	1.00	1.24	1.47	1.78	2.13	2.45	2.82	3.17	3.50
	x_{hs}	0.01	0.02	0.03	0.05	0.08	0.13	0.18	0.25	0.32	0.40	0.49
YbZn	μ_{eff}	4.53	4.53	4.54	4.54	4.54	4.54	4.54	4.54	4.56	4.55	4.53
YbFe	μ_{eff}	4.58	4.59	4.63	4.69	4.77	4.86	5.02	5.10	5.26	5.43	5.63
	$\mu_{eff}(Fe)$	0.60	0.75	0.93	1.16	1.47	1.72	2.08	2.32	2.62	2.97	3.35
	x_{hs}	0.01	0.02	0.03	0.05	0.08	0.11	0.16	0.22	0.29	0.36	0.44

[a] μ_{eff} are corrected for diamagnetic contributions (see text); estimated error is typically $\pm$ 0.03 μ_B. [b] Calculated according to equation (6).

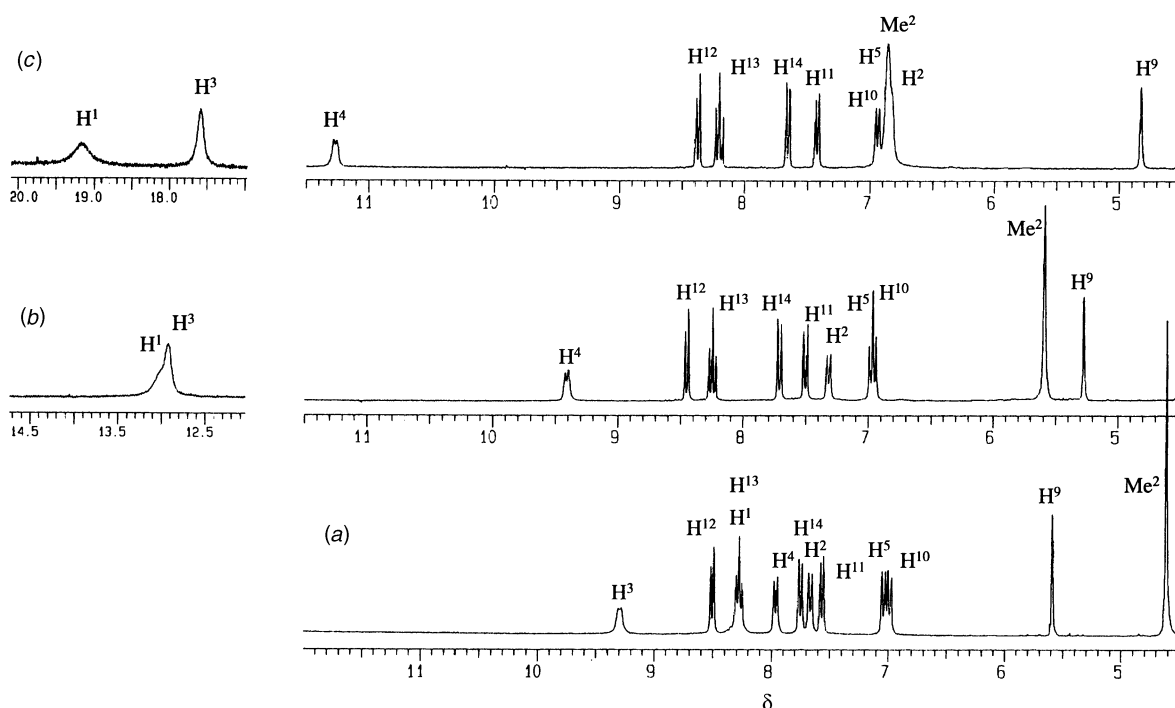**Fig. 4** Aromatic part of the ^1H NMR spectra of $[LaFeL^4_3]^{5+}$ at (a) 233, (b) 273 and (c) 298 K in CD_3CN. Complex concentration: 8 mmol dm^{-3}

molecular interactions occur in solution and taking into account the mixing entropy,[45] the spin-crossover constant K_{sc} and the mole fraction of high-spin Fe^{II} (x_{hs}) may be calculated according to equation (5)[45,46] where μ_{ls} and μ_{hs} are respectively

$$K_{sc}(T) = \exp\left(-\frac{\Delta H_{sc}}{RT} + \frac{\Delta S_{sc}}{R}\right) = \frac{x_{hs}}{1 - x_{hs}} = \frac{\mu_{eff}^2 - \mu_{ls}^2}{\mu_{hs}^2 - \mu_{eff}^2} \quad (5)$$

the effective magnetic moments for the low-spin (0.3 μ_B) and high-spin forms (5.0 μ_B).[50] The mole fractions x_{hs} evidence a smooth and incomplete spin transition corresponding to the existence of almost pure low-spin complexes at 233 K and leading to ca. 40–50% of high-spin complexes at 333 K (Table 4,

Fig. 5). Plots of ln (K_{sc}) vs. T^{-1} are linear (correlation coefficients between 0.9974 and 0.9993) except that for $[ScFeL^4_3]^{3+}$ which is only linear between 283 and 333 K. Below 283 K we observe a significant deviation from linearity corresponding to unexpectedly large μ_{eff} associated with partial decomplexation of $[ScFeL^4_3]^{5+}$ observed by ^1H NMR spectroscopy at low temperature (see above). The estimated values of ΔH_{sc} and ΔS_{sc} extracted from these linear plots are reported in Table 5 and predicted values of x_{hs} calculated according to equation (5) are shown together with the experimental data in Fig. 5. The parameter ΔH_{sc} is dominated by the inner-sphere reorganization energy associated with the elongation of the Fe–N bonds (0.11–0.24 Å)[22,43,45] and is ca. 7–9 kJ mol^{-1} larger than those obtained

Table 5 Thermodynamic parameters for $^1A_1 \longleftrightarrow {}^5T_2$ spin-state equilibria of $[LnFeL^4_3][ClO_4]_5$ and $[CaFeL^4_3][ClO_4]_4$ in MeCN obtained from magnetic measurements

Compound	$\Delta H_{sc}/$ kJ mol^{-1}	$\Delta S_{sc}/$J K^{-1} mol^{-1}	$T_c{}^a$/K	σ^b	R^c/Å
$[CaFeL^4_3]^{4+}$	30.3(3)	90(1)	336	0.9990	1.18
$[LaFeL^4_3]^{5+}$	30.5(3)	92(1)	331	0.9993	1.216
$[NdFeL^4_3]^{5+}$	30.2(3)	90(1)	334	0.9991	1.163
$[EuFeL^4_3]^{5+}$	29.6(5)	89(1)	336	0.9979	1.12
$[YFeL^4_3]^{5+}$	29.6(3)	88(1)	338	0.9991	1.075
$[YbFeL^4_3]^{5+}$	28.3(4)	83(1)	342	0.9982	1.042
$[LuFeL^4_3]^{5+}$	28.4(4)	82(2)	346	0.9980	1.032
$[ScFeL^4_3]^{5+}$	25.8(7)	74(2)	349	0.9974	0.925^d

^{a} Critical temperature for which $x_{hs} = 0.5$ ($T_c = \Delta H_{sc}/\Delta S_{sc}$).[45] ^{b} Correlation coefficients for plots of ln K_{sc} vs. T^{-1} (see text). ^{c} Effective ionic radii for nine-co-ordinate Ln^{III} and Ca^{II}.[44] ^{d} Extrapolated effective ionic radius of nine-co-ordinate Sc^{III}; $R(Sc^{III}) = R(Y^{III}) - 0.15$ Å.[35]
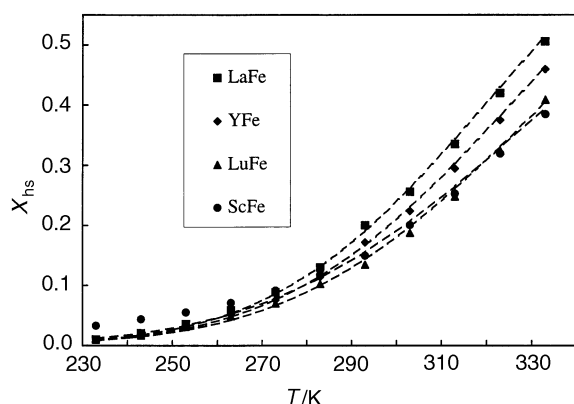
Fig. 5 Mole fraction of high-spin Fe^{II} in $[LnFeL^4_3]^{5+}$ (Ln = La, Lu, Y or Sc) in MeCN. Dashed curves correspond to predicted data using the thermodynamic parameters of Table 5

for $[LnFeL^3_3]^{5+}$ (Ln = La–Eu, 20–23 kJ mol^{-1})[18] and $[FeL^5_3]^{2+}$ (21.4 kJ mol^{-1} in MeCN–MeOH),[32] which strongly suggests that the co-ordination of Ln^{III} by the three tridentate units in $[MFeL^4_3]^{5+}$ significantly limits the required expansion of the iron(II) co-ordination sphere when going from low- to high-spin Fe^{II}. A careful examination of Table 5 shows that the thermodynamic parameters ΔH_{sc} and ΔS_{sc} are correlated with the effective ionic radii of Ln^{III}, the larger lanthanides producing larger ΔH_{sc} and ΔS_{sc}, and resulting in a limited increase of the critical temperature T_c (at which $x_{hs} = 0.5$) for the smaller lanthanide(III) ions.

In order to confirm this hypothesis, paramagnetic Ln^{III} of intermediate sizes (Nd, Eu and Yb) have been considered. As a result of the ineffective overlap between the 4f and the ligand or the 3d orbitals,[51] the isotropic interaction parameter J is weak in heteronuclear d–f complexes ($J < 10$ cm^{-1}).[52] It may be neglected in our case since (i) there is no short-distance bridging ligand (the La$\cdots$Fe distance in **11** is 9.029 Å) and (ii) $kT \gg |J|$ for the temperature range accessible in acetonitrile (233–333 K). Thus Fe^{II} and Ln^{III} were considered as being two independent paramagnetic centres, as recently reported for heterodinuclear LnCu complexes.[53] The paramagnetic moments of Ln^{III} were taken from the analogous complexes $[LnZnL^4_3]^{5+}$ which display the expected Curie magnetic behaviour for Ln = Nd and Yb [$\mu_{eff} = 3.56(3)$ and $4.54(3)$ respectively] and the particular non-Curie behaviour for Eu^{III} resulting from the thermal population of the $^7F_{1-3}$ excited states (a fit with a spin–orbit coupling constant between 310 and 320 cm^{-1} is satisfactory).[45] The magnetic moments of Fe^{II} (Table 4) were then calculated according to equation (6). The spin-state equilibrium parameters ΔH_{sc}

$$\mu_{eff}(Fe) = \sqrt{\mu_{eff}^2(LnFe) - \mu_{eff}^2(LnZn)} \tag{6}$$

and ΔS_{sc} confirm the correlation with the effective ionic radii of Ln^{III} (Table 5). The ΔS_{sc} values (74–92 J mol^{-1} K^{-1}) correspond to large entropic contributions compared to those of $[LnFeL^3_3]^{5+}$ (55–66 J mol^{-1} K^{-1}), but they are similar to those reported for other bidentate α,α'-diimine ligands in $[FeL^5_3]^{2+}$ (92 J mol^{-1} K^{-1})[32] and $[FeL_3]^{2+}$ (83–97 J mol^{-1} K^{-1}),[54] where L is a substituted bidentate 2-pyridyl-1,2,4-triazole ligand. The origin of the variation of ΔS_{sc} is not trivial since several processes contribute to the entropy term (electronic, vibrational partition functions, outer-sphere reorganisation of the solvent cage),[22,43,45] but the monotonous increase of ΔS_{sc} and ΔH_{sc} associated with the decrease in the effective ionic radii of the co-ordinated Ln^{III} in $[LnFeL^4_3]^{5+}$ indicates that both parameters are influenced by the nature of the lanthanide ion.

The molar absorption coefficients of the pure low- (ε_{ls}) and high-spin (ε_{hs}) $[LnFeL^4_3]^{5+}$ complexes were estimated from the calculated x_{hs} given in Table 4, using equation (7). Straight lines

$$\varepsilon^\lambda_{tot} = \varepsilon^\lambda_{ls} - x_{hs}(\varepsilon^\lambda_{ls} - \varepsilon^\lambda_{hs}) \tag{7}$$

of ε_{tot} vs. x_{hs} were found at all wavelengths, leading to a maximum for the m.l.c.t. band envelope of the low-spin form at around 18 900–19 000 cm^{-1}. The high-spin form does not show any pronounced maximum in the range 14 500–23 000 cm^{-1} and typical spectra are shown in Fig. 3 for $[LaFeL^4_3]^{5+}$.

Solid-state structure of $[LnFeL^4_3][ClO_4]_5$

Slow diffusion of diethyl ether into concentrated acetonitrile solutions of $[LnFeL^4_3]^{5+}$ produces almost quantitative yield of deep red microcrystalline aggregates, the elemental analyses of which correspond to the formulae $[LnFeL^4_3][ClO_4]_5 \cdot 0.5Et_2O \cdot nH_2O$ ($n = 1$, Tb **5**; $n = 2$, Ln = La **1**, Eu **3**, Gd **4**, Lu **7** or Y **8**). Their IR spectra are similar to those of $[LnZnL^4_3][ClO_4]_5$ and show ionic perchlorates.[20] We were unable to obtain crystals suitable for X-ray diffraction studies with perchlorate anions, but small and extremely fragile deep red crystals of $[LaFeL^4_3][ClO_4]_{0.5}[CF_3SO_3]_{4.5} \cdot MeCN \cdot 4H_2O$ **11** are obtained from solutions of **1** containing 30 equivalents of $[NBu_4]-[O_3SCF_3]$. When isolated from the mother-liquor the prisms quickly transform into a microcrystalline powder, the elemental analysis and IR spectrum of which are compatible with loss of the acetonitrile molecule. Attempts to grow suitable crystals with Eu^{III} instead of La^{III} led to isostructural, but more disordered complexes.
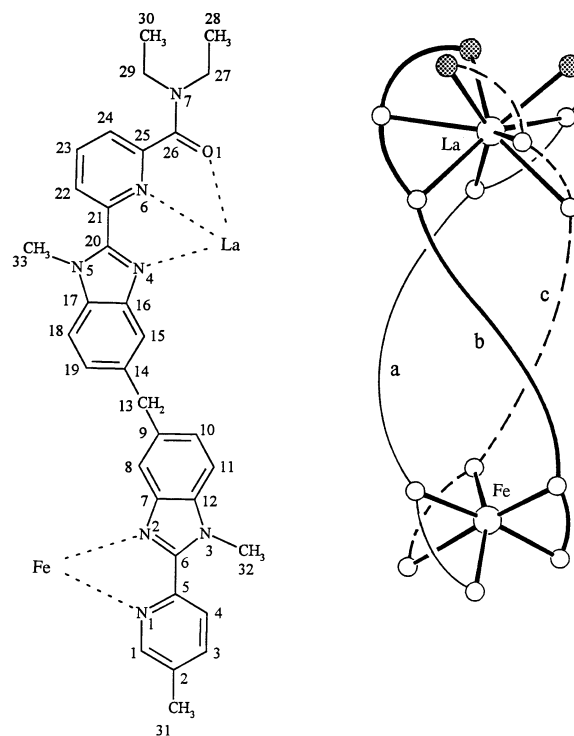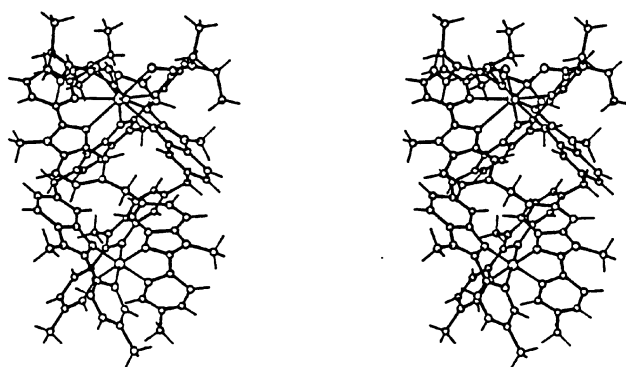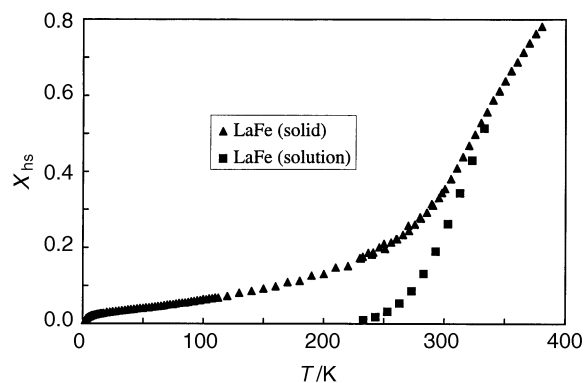
$[LaFeL^4_3][ClO_4]_{0.5}[CF_3SO_3]_{4.5} \cdot MeCN \cdot 4H_2O$ **11.** The crystal structure of complex **11** has been determined at 170 K to minimize the fraction of high-spin Fe^{II} and consists of low-spin cations $[LaFeL^4_3]^{5+}$, unco-ordinated perchlorate and triflate (trifluoromethanesulfonate) anions and solvent molecules. The anions and solvent molecules are disordered, which limits the accuracy of the structural determination. The complex is isostructural with $[EuZnL^4_3][ClO_4][CF_3SO_3]_4 \cdot 4MeCN$ (see Experimental section).[19,20] In the cation $[LaFeL^4_3]^{5+}$ three head-to-head ligand strands are wrapped around the metal ions defining a pseudo-C_3 axis and confirming the structure found in solution. Fig. 6 shows the atom numbering scheme, and Fig. 7 gives a stereoscopic ORTEP[55] view of the cation while selected bond distances and angles are reported in Table 6.

The La^{III} atom lies in the pseudo-ttp site produced by the three-co-ordinated tridentate units, the three central nitrogen atoms of the pyridine rings occupying the capping positions which form an intermediate plane almost containing the metal (deviation 0.08 Å). The La–N (2.59–2.69 Å) and the La–O bonds (2.47–2.50 Å) are ca. 7% longer than those observed around Eu^{III} in $[EuZnL^4_3]^{5+}$[20] leading to an effective ionic radius for La^{III} of 1.21 Å according to Shannon's definition [$r(N) = 1.46$, $r(O) = 1.31$ Å],[44] in good agreement with the expected value of 1.216 Å.[44] Although the smaller low-spin Fe^{II}

Table 6 Selected bond distances (Å) and angles (°) for complex **11**

		Ligand		
		a	b	c
La···Fe	9.029(4)			
La–O(1)		2.49(2)	2.47(2)	2.50(2)
La–N(4)		2.68(2)	2.69(2)	2.67(2)
La–N(6)		2.69(2)	2.67(2)	2.59(2)
Fe–N(1)		1.96(2)	2.04(2)	2.00(2)
Fe–N(2)		1.98(2)	1.95(2)	1.93(2)
Bite angles				
N(1)–Fe–N(2)		82.1(9)	79(1)	78.8(9)
N(4)–La–N(6)		59.5(6)	59.1(7)	60.6(6)
N(6)–La–O(1)		61.4(6)	62.6(6)	61.9(6)

N–Fe–N

N(1a)–Fe–N(2b)	87.7(9)	N(1a)–Fe–N(1c)	96.1(9)
N(1a)–Fe–N(2c)	174.9(9)	N(2a)–Fe–N(1b)	175.8(9)
N(2a)–Fe–N(2b)	97.4(8)	N(2a)–Fe–N(1c)	85.6(8)
N(2a)–Fe–N(2c)	96.9(8)	N(1a)–Fe–N(1b)	95.0(9)
N(1b)–Fe–N(1c)	98(1)	N(1b)–Fe–N(2c)	86.2(9)
N(2b)–Fe–N(1c)	175.5(9)	N(2b)–Fe–N(2c)	97.4(9)

N–La–N

N(4a)–La–N(4b)	91.9(6)	N(6a)–La–N(6b)	122.5(7)
N(4b)–La–N(4c)	88.3(6)	N(6b)–La–N(6c)	116.0(7)
N(4a)–La–N(4c)	89.5(6)	N(6a)–La–N(6c)	121.2(7)
N(4a)–La–N(6c)	145.3(6)	N(4a)–La–N(6b)	77.1(7)
N(6a)–La–N(4b)	146.5(7)	N(4b)–La–N(6c)	71.7(6)
N(6b)–La–N(4c)	143.7(6)	N(6a)–La–N(4c)	75.4(6)

O–La–N

N(4a)–La–O(1c)	146.7(6)	N(4a)–La–O(1b)	76.4(6)
N(6a)–La–O(1b)	71.5(6)	N(6a)–La–O(1c)	133.7(6)
N(6b)–La–O(1c)	70.9(7)	N(4b)–La–O(1c)	79.8(6)
O(1a)–La–N(6b)	137.6(7)	O(1a)–La–N(4a)	120.8(6)
O(1a)–La–N(4c)	78.1(6)	O(1a)–La–N(6c)	72.5(6)
O(1c)–La–N(4c)	122.1(6)	O(1a)–La–N(4b)	144.0(6)
O(1b)–La–N(4c)	146.7(5)	O(1b)–La–N(6c)	138.2(6)
O(1b)–La–N(4b)	121.6(6)		

O–La–O

O(1a)–La–O(1b)	83.5(6)	O(1b)–La–O(1c)	80.7(5)
O(1a)–La–O(1c)	79.7(6)		

Fig. 6 Atomic numbering scheme for $[LaFeL^4_3]^{5+}$ in complex **11**

Fig. 7 An ORTEP stereoview[55] of the cation $[LaFeL^4_3]^{5+}$ perpendicular to the psuedo-C_3 axis

Fig. 8 Mole fraction of high-spin Fe^{II} for $[LaFeL^4_3]^{5+}$ in the solid state and in solution

has replaced Zn^{II} in going from $[EuZnL^4_3]^{5+}$ to $[LaFeL^4_3]^{5+}$, no severe structural constraints are evidenced around Ln^{III} and similar lanthanide co-ordination sites are found in both structures, except for a slightly larger twist angle between the two opposite facial tripods of the trigonal prism in $[LaFeL^4_3]^{5+}$ ($\omega = 17°$) compared to $\omega = 10°$ for EuZn (perfect trigonal prism, $\omega = 0$; perfect octahedron, $\omega = 60°$; SUP 57202).[20] A related effect has been reported for the pseudo-ttp site of $[Ln(pydca)_3]^{3-}$ (pydca = pyridine-2,6-dicarboxylate) where the two tripods are almost eclipsed for Ln = Lu and significantly staggered for Ln = La.[56] The three remaining bidentate units provide a slightly distorted pseudo-octahedral co-ordination site around Fe^{II}. The Fe–N bond distances lie in the range 1.93–2.04 Å (average 1.98 Å) which is typical for d^6 low-spin Fe^{II} (1.96–2.03 Å).[22] As a result of bite angles significantly shorter than 90° (79–82°), the co-ordination sphere around Fe^{II} is best described as a slightly flattened octahedron along the C_3 axis (SUP 57202). The average θ angle amounts to 60°, a value slightly larger than the 54.7° expected for a perfect octahedron,[16,57] and the average angle ω_i between two Fe–N bonds of the different facial tripods of the pseudo-octahedron amounts to 55°, similar to the expected 60° for a perfect octahedron, in good agreement with the proposed low-spin iron(II) electronic configuration since a larger deformation is expected for high-spin Fe^{II}.[22,58] Compared to the strongly distorted co-ordination sphere observed for Zn^{II} in $[EuZnL^4_3]^{5+}$,[19,20] the stereochemically demanding d^6 low-spin Fe^{II}[58] strongly limits the geometrical deformation of the pseudo-octahedral co-ordination site, but

the intermetallic distance is not significantly altered (Eu···Zn, 8.960; La···Fe, 9.029 Å). As described for $[EuZnL^4_3]^{5+}$,[20] the $[LaFeL^4_3]^{5+}$ cations are packed by pairs of opposite helicites in the unit cell leading to a rather short intermolecular Fe···Fe distance (9.700 Å).

Iron(II) spin crossover of $[LnFeL^4_3]^{5+}$ (Ln = La 1, Lu 7 or Y 8) in the solid state

The effective paramagnetic moments point to a smooth spin transition in the range 150–380 K (Fig. 8). The transition is *ca.* 80% complete at 380 K, but we observe an incomplete formation of low-spin Fe^{II} at low temperature leading to residual magnetic moments corresponding to *ca.* 8% of high-spin Fe^{II} at 150 K. No hysteresis is observed between the heating and cooling processes which implies only weak intermolecular interactions between the iron(II) centres.[45] However, plots of ln $[x_{hs}/(1-x_{hs})]$ *vs.* T^{-1} are not linear preventing the simple estimation of ΔH_{sc} and ΔS_{sc} and suggesting that minor intermolecular interactions and/or partial inhomogeneity in the isolated materials are responsible for the deviation from the regular spin-crossover behaviour observed in solution.[45]

Photophysical properties of $[LnFeL^4_3][ClO_4]_5 \cdot 0.5Et_2O \cdot nH_2O$ (n = 1, Tb 5; n = 2, Ln = La 1, Eu 3, Gd 4 or Lu 7) in the solid state

Upon complexation, the intense $\pi \longrightarrow \pi^*$ transitions centred on L^4 are red-shifted by *ca.* 1400 cm^{-1} and a new band appears around 19 000 cm^{-1} which is assigned to the m.l.c.t. transition as previously described for $[LnFeL^4_3]^{5+}$ in solution. Excitation of complexes **1**, **4** and **7** in the UV (308 nm) produces a faint ligand-centred luminescence with maxima at 22 220 and 18 520 cm^{-1} which contrasts with the well resolved emission spectra observed for the analogous complexes $[LnZnL^4_3][ClO_4]_5$ (Ln = La, Gd or Lu)[20] and indicates that efficient quenching processes employing the m.l.c.t. and d–d excited states occur when Zn^{II} is replaced by Fe^{II}, *cf.* $[LnFeL^3_3][ClO_4]_5$.[18] The Eu-containing complex **3** is even less luminescent and no emission from the ligand or from Eu ($^5D_0$) can be detected for temperatures in the range 10–400 K which means that a ligand to europium energy transfer occurs, but subsequent quenching processes deactivate the Eu-centred emission. Since the analogous $[EuZnL^4_3]^{5+}$ complex is strongly luminescent,[19,20] we assume that the m.l.c.t. and/or the 3d states associated with low- and high-spin Fe^{II} are responsible for the efficient quenching.

Conclusion

The replacement of Zn^{II} by Fe^{II} does not dramatically affect the assembly process and triple-helical non-covalent lanthanide podates $[LnFeL^4_3]^{5+}$ similar to $[LnZnL^4_3]^{5+}$ [19,20] are obtained in solution and in the solid state. In these supramolecular complexes the d-block ion occupies the facial six-co-ordinate site produced by the three bidentate binding units which organize the tridentate units for their co-ordination to the nine-co-ordinate Ln^{III}. The 17% contraction of the effective ionic radius when going from Zn^{II} to low-spin Fe^{II} has only little influence on the co-ordination site occupied by Ln^{III} as judged by the similarity between the NMR and the X-ray diffraction data of $[LnML^4_3]^{5+}$ (M = Fe or Zn). However, the crystal structure of $[LaFeL^4_3]^{5+}$ demonstrates that the small and stereochemically demanding low-spin Fe^{II} enforces some constraints at the pseudo-octahedral site. In solution, electrochemical and spectroscopic data confirm that Fe^{II} lies in a flattened pseudo-octahedral site, but accurate magnetic measurements using Fe^{II} as a magnetic probe[18] clearly establish that the size of the 4f-block ion in the nine-co-ordinate site produces significant structural constraints in the six-co-ordinate site occupied by the 3d ion. Consequently, the thermodynamic parameters of the iron(II) spin-state equilibria may be finely controlled by Ln^{III} in $[LnFeL^4_3]^{5+}$ leading to a limited tuning of the critical temperature. However, a synergetic electronic influence of the 3d metal on the 4f ion is evidenced by the strong europium luminescence observed for $[EuZnL^4_3]^{5+}$ which is completely quenched for $[EuFeL^4_3]^{5+}$. The stability of the final supramolecular complexes also depends on the pair of metal ions and for a given lanthanum(III) ion the $[LnFeL^4_3]^{5+}$ podates are significantly less stable than the structurally analogous $[LnZnL^4_3]^{5+}$ complexes while intricate mixtures are obtained in solution when Ln^{III} are replaced by the smaller Sc^{III} and Al^{III}. Such synergetic effects on the structural, spectroscopic and magnetic properties between the two different metal ions in the heterodinuclear organized architectures offer fascinating possibilities for the development of supramolecular devices if suitable external stimuli may induce specific responses.[59] The thermally induced iron(II) spin transitions in $[LnFeL^4_3]^{5+}$ represent a first step toward this goal, but lower critical temperatures (T_c) are required for investigating the possible luminescent response of the associated Ln^{III}. Suitable modifications of the bidentate binding units of the ligands are currently under investigation together with the development of directional d–f light-converting devices.

Experimental

Solvents and starting materials

These were obtained from Fluka AG (Buchs, Switzerland) and used without further purification unless otherwise stated. Acetonitrile was distilled twice from CaH_2 and the pro-ligand 2-[6-(diethylcarbamoyl)pyridin-2-yl]-1,1′-dimethyl-2′-(5-methyl-pyridin-2-yl)-5,5′-methylenebis(1*H*-benzimidazole) (L^4) was prepared according to a literature procedure.[20] The perchlorate salts Ln(ClO$_4$)$_3 \cdot n$H$_2$O (Ln = La, Nd, Eu, Gd, Tb, Yb, Lu, Y or Sc; n = 6–8) were prepared from the corresponding oxides[60] (Glucydur, 99.99%); Ca(ClO$_4$)$_2 \cdot$H$_2$O was obtained by metathesis of CaCO$_3$ with aqueous perchloric acid.

Preparations

$[LnFeL^4_3][ClO_4]_5 \cdot 0.5Et_2O \cdot nH_2O$ (n = 1, Ln = Tb 5; n = 2, Ln = La 1, Eu 3, Gd 4, Lu 7 or Y 8). A solution of Ln(ClO$_4$)$_3 \cdot n$H$_2$O (18.4 µmol) (Ln = La, Eu, Gd, Tb, Lu or Y) and Fe(ClO$_4$)$_2 \cdot$6H$_2$O (6.68 mg, 18.4 µmol) in acetonitrile (2 cm^3) was slowly added to a solution of L^4 (30 mg, 55.2 µmol) in CH$_2$Cl$_2$–MeCN (1:1, 5 cm^3). After stirring for 1 h at room temperature, the solution was evaporated, the solid residue dissolved in MeCN (3 cm^3) and Et$_2$O was diffused into the solution for 3 d. The resulting deep red microcrystalline aggregates were filtered off and dried to give 85–95% of complexes $[LnFeL^4_3]$-$[ClO_4]_5 \cdot 0.5Et_2O \cdot nH_2O$ (n = 1, Tb 5; n = 2, Ln = La 1, Eu 3, Gd 4, Lu 7 or Y 8). X-Ray-quality prisms of $[LaFeL^4_3][ClO_4]_{0.5}$-$[CF_3SO_3]_{4.5} \cdot MeCN \cdot 4H_2O$ **11** were obtained by slow diffusion of Et$_2$O into a MeCN solution of **1** containing 30 equivalents of [NBu$_4$][O$_3$SCF$_3$]. When separated from the mother-liquor, the prisms are readily transformed into a microcrystalline powder the elemental analysis (Table 7) and IR spectrum of which are compatible with the formulation $[LaFeL^4_3][ClO_4]_{0.5}[CF_3SO_3]_{4.5} \cdot 4H_2O$ **12**.

$[LnFeL^4_3][ClO_4]_5$ (Ln = Nd 2, Yb 6 or Sc 9) and $[CaFeL^4_3]$-$[ClO_4]_4$ **10**. These complexes were prepared *in situ* for ^{1}H NMR

Table 7 Elemental analyses for complexes **1**, **3–5**, **7**, **8** and **12**

| Complex | Analysis (%)* | | |
	C	H	N
1	50.6 (50.6)	4.5 (4.5)	12.3 (12.3)
3	50.4 (50.4)	4.4 (4.5)	12.2 (12.2)
4	50.5 (50.2)	4.5 (4.5)	12.2 (12.2)
5	50.5 (50.6)	4.4 (4.5)	12.3 (12.3)
7	50.2 (49.9)	4.5 (4.5)	12.1 (12.1)
8	51.9 (51.7)	4.6 (4.6)	12.5 (12.5)
12	48.0 (47.5)	4.1 (4.1)	11.1 (11.2)

* Calculated values in parentheses.

and magnetic studies. An equimolar 0.02 mol dm^{-3} solution of Ln(ClO$_4$)$_3$·nH$_2$O (Ln = Nd, Yb or Sc) or Ca(ClO$_4$)$_2$·H$_2$O and Fe(ClO$_4$)$_2$·6H$_2$O in acetonitrile (280 μl, 5.6 μmol) was added to L^4 (9.1 mg, 16.8 μmol) dissolved in dichloromethane–acetonitrile (1:1, 4 cm^3) under an inert atmosphere. After evaporation the solid residue was dried under vacuum, then dissolved in degassed CD$_3$CN (700 μl) + 1% SiMe$_4$ to give 8 mmol dm^{-3} of [LnFeL$^4_3$][ClO$_4$]$_5$ (Ln = Nd **2**, Yb **6** or Sc **9**) and [CaFeL$^4_3$][ClO$_4$]$_4$ **10**, the purity of which was checked by ^{1}H NMR spectroscopy.

CAUTION: perchlorate salts with organic ligands are potentially explosive and should be handled with the necessary precautions.[61]

Crystallography

Fragile crystals of [LaFeL$^4_3$][ClO$_4$]$_{0.5}$[CF$_3$SO$_3$]$_{4.5}$·MeCN·4H$_2$O **11** were prepared as previously described and mounted from the mother-liquor on a quartz fibre with perfluoropolyether oil RS3000.

Crystal data. C$_{105.5}$H$_{110}$Cl$_{0.5}$F$_{13.5}$FeLaN$_{22}$O$_{22.5}$S$_{4.5}$, $M = 2659.4$, monoclinic, space group $C2/c$, $a = 51.369(6)$, $b = 20.650(4)$, $c = 23.928(4)$ Å, $\beta = 90.342(8)°$, $U = 25382(7)$ Å^3 [by least-squares refinement of 24 reflections (30 $\leqslant$ 2θ $\leqslant$ 45°)], $Z = 8$, $D_c = 1.39$ g cm^{-3}, $F(000) = 10\,896$. Deep red prisms. Crystal dimensions 0.26 × 0.30 × 0.34 mm, μ(Cu-Kα) = 5.065 mm^{-1}.

Data collection and processing. Nonius CAD4 diffractometer, $T = 170$ K, ω–2θ mode with ω scan width = 1.5 + 0.14 tan θ, ω-scan speed 0.137° s^{-1}, Cu-Kα radiation ($\lambda = 1.5418$ Å); 13421 reflections measured (4 $\leqslant$ 2θ $\leqslant$ 100°, $-50 < h < 50$, $0 < k < 20$, $0 < l < 23$), 13027 unique reflections (R_{int} for equivalent reflections = 0.087) of which 7294 were observable [$|F_o| > 4\sigma(F_o)$]. Two reference reflections were measured every 30 min and showed a total decrease in intensity of 5.5%. All intensities were corrected for this drift.

Structure analysis and refinement. Data were corrected for Lorentz-polarization and absorption effects[62] ($A^*_{min} = 2.651$, $A^*_{max} = 5.809$). The structure was solved by direct methods using MULTAN 87;[63] all other calculations used the XTAL[64] system and ORTEP II[55] programs. Full-matrix least-squares refinements (on F) gave final values of $R = R' = 0.126$ ($w = 1$) for 1378 variables and 7294 contributing reflections. The carbon, fluorine and oxygen atoms of the triflate anions and of the water molecules were refined with isotropic displacement parameters (38 atoms) and all the other atoms (135) with anisotropic displacement parameters. A careful analysis of the anisotropy of the U values showed a weak flipping of the terminal pyridine rings [N(1), C(1)–C(5)] roughly perpendicular to the aromatic plane. Triflate f is disordered and was refined with two distinct orientations of the fluorine atoms (population parameter, PP = 0.5; for site occupancy factors, see SUP 57202). The perchlorate anion and the O$_3$SC group of triflate d occupy the same site and were refined as ClO$_4$ (with PP = 1) and the remaining three fluorine atoms with PP = 0.5. All the anions were refined with restraints on bond distances and angles. The mean shift/error on the last cycle was 0.0064 and the maximum 0.183. Hydrogen atoms were placed in calculated positions and contributed to F_c calculations. The final Fourier-difference synthesis showed a maximum of +1.71 and a minimum of −2.07 e Å^{-3} located around the La atom. Complex **11** is isostructural with [EuZnL$^4_3$][ClO$_4$][CF$_3$SO$_3$]$_4$·4MeCN.[20] In order to keep the monoclinic angle β larger than 90° in **11**, correspondence between the two data sets was obtained by a transformation of the unit cell ($\bar{a}, \bar{b}, c$) together with an origin shift of (0,$\frac{1}{2}$,$\frac{1}{2}$).

Atomic coordinates, thermal parameters, and bond lengths

Spectroscopic and analytical measurements

Electronic spectra were recorded at 20 °C from 10^{-3} mol dm^{-3} solutions in MeCN with Perkin-Elmer Lambda 5 and Lambda 7 spectrometers using quartz cells of 0.1 and 0.01 cm path length. Spectrophotometric titrations were performed with a Perkin-Elmer Lambda 5 spectrophotometer connected to an external computer. In a typical experiment, compound L^4 in acetonitrile (10^{-4} mol dm^{-3}, 50 cm^3) was titrated at 20 °C with an equimolar solution of Ln(ClO$_4$)$_3$·nH$_2$O and Fe(ClO$_4$)$_2$·6H$_2$O (0.83 mmol dm^{-3}) in MeCN. After each addition of 0.20 cm^3 the absorbances at 10 wavelengths were recorded using a 0.1 cm quartz cell and transferred to the computer. Factor analysis and stability-constant determination were carried out as previously described.[29] Infrared spectra were obtained from KBr pellets with a Perkin-Elmer 883 spectrometer, ^{1}H NMR spectra at 25 °C on a Broadband Varian Gemini 300 spectrometer. Chemical shifts are given in ppm with respect to SiMe$_4$. Electron-impact mass spectra (70 eV) were recorded with VG-7000E and Finnigan-4000 instruments. Pneumatically assisted electrospray mass spectra were recorded from 10^{-4} mol dm^{-3} acetonitrile solutions on API III and API 300 tandem mass spectrometers (PE Sciex) by infusion at 4–10 μl min^{-1}, under low up-front declustering or collision-induced dissociation (CID) conditions, typically $\Delta V = 0$–30 V between the orifice and the first quadrupole of the spectrometer.[26] The total charge (z) of the complexes was determined by using the isotopic pattern ($z \leqslant 3$) or adduct ions with perchlorate anions ($z > 3$).[26] The experimental procedures for high-resolution, laser-excited luminescence measurements have been published previously.[65] Cyclic voltammograms were recorded using a BAS CV-50W potentiostat connected to a personal computer. A three-electrode system consisting of a stationary platinum disc working electrode, a platinum counter electrode and a non-aqueous Ag–AgCl reference electrode was used; NBu$_4$PF$_6$ (0.1 mol dm^{-3} in MeCN) served as an inert electrolyte. The reference potential ($E^o = -0.12$ V *vs.* SCE) was standardized against [Ru(bipy)$_3$]-[ClO$_4$]$_2$ (bipy = 2,2′-bipyridyl).[66] The scan speed was 100 mV s^{-1} and voltammograms were analysed according to established procedures.[66] Elemental analyses were performed by Dr. H. Eder from the Microchemical Laboratory of the University of Geneva.

Magnetic measurements

Magnetic data for samples in acetonitrile were obtained by the Evans method[46] using a Varian Gemini 300 spectrometer and the solvent methanol for temperature calibration.[67] The method was modified according to Baker *et al.*[47] for application with a superconducting magnet ($S_f = 4\pi/3$ for a cylindrical sample parallel to the magnetic field). Specific problems associated with the 'solvent correction term'[48] were overcome by determining the diamagnetic contribution under the same experimental conditions.[49] Measurements were carried out on degassed CD$_3$CN solutions containing 8 × 10^{-3} mol dm^{-3} complex and 1% (v/v) SiMe$_4$ as an internal reference. All the data were corrected for changes in solvent density with temperature.[68] The diamagnetic contributions of the ligand L^4 and the perchlorate anions in the heterodinuclear complexes [LnFeL$^4_3$][ClO$_4$]$_5$ were obtained from the molar diamagnetic susceptibility measured for [LaZnL$^4_3$][ClO$_4$]$_5$ with the Evans method ($m^{dia} = 0.0325$ g cm^{-3}, $\delta\nu^{dia} = -7.1$ Hz). Molar paramagnetic susceptibilities of [LnFeL$^4_3$][ClO$_4$]$_5$ were measured at 10 K intervals between 233 and 333 K, corrected for diamagnetism and converted into effective magnetic moments μ$_{eff}$ according to equation (8)[49]

$$\mu_{\text{eff}} = 2.828 \sqrt{\frac{T}{\nu_0 S_f} \cdot \left(\frac{\delta \nu^p M^p}{m^p} - \frac{\delta \nu^{\text{dia}} M^{\text{dia}}}{m^{\text{dia}}} \right)} \qquad (8)$$

where m^p and m^{dia} are the concentrations of the paramagnetic solute and its diamagnetic analogue respectively (g cm^{-3}), $\delta\nu^p$ and $\delta\nu^{\text{dia}}$ the chemical shift differences (Hz) between the resonances of the reference compound in the two coaxial tubes ($\delta\nu > 0$ for paramagnetism, < 0 for diamagnetism),[46] M^p and M^{dia} the molecular masses of the paramagnetic and diamagnetic compounds respectively (g mol^{-1}), T is the absolute temperature, μ_{eff} the effective magnetic moment (μ_B) and S_f the shape factor of the magnet.[47]

To check for complications associated with possible partial decomplexation,[69] the magnetic susceptibilities of [LaFeL$^4_3$]-[ClO$_4$]$_5$ were recorded for total ligand concentrations between 1.5 and 2.5×10^{-2} mol dm^{-3} at each temperature (233–333 K). No significant variation of μ_{eff} was observed within experimental error, which confirms the ^{1}H NMR data and demonstrates that [LaFeL$^4_3$]$^{5+}$ is the only species formed in solution. All subsequent magnetic measurements were obtained from solutions containing 8×10^{-3} mol dm^{-3} of complexes.

Solid-state volume magnetic susceptibilities of complexes **1**, **3**, **7** and **8** were obtained with a model MPMS5 SQUID magnetometer Quantum Design operating at a magnetic field strength of 3000 Oe, in the range 1.9–380 K for **1** and 1.9–300 K for **7** and **8**. The data were corrected for diamagnetism using [LaZnL$^4_3$][ClO$_4$]$_5 \cdot 0.5$Et$_2$O$\cdot 2$H$_2$O [$\chi^{\text{dia}} = -4.67(9) \times 10^{-4}$ cm^3 mol^{-1}] and for paramagnetic iron(III) impurities (0.5–2%) before conversion into effective magnetic moments.[69]

Acknowledgements

References

1 J.-C. G. Bünzli, in *Lanthanide Probes in Life, Chemical and Earth Sciences*, eds. J.-C. G. Bünzli and G. R. Choppin, Elsevier, Amsterdam, 1989, ch. 7; J.-C. G. Bünzli, P. Froidevaux and C. Piguet, *New J. Chem.*, 1995, **19**, 661 and refs. therein.

2 J.-C. G. Bünzli and J.-M. Pfefferlé, *Helv. Chim. Acta*, 1994, **77**, 323; F. S. Richardson, *Chem. Rev.*, 1982, **82**, 541; P. R. Selvin, T. M. Rana and J. E. Hearst, *J. Am. Chem. Soc.*, 1994, **116**, 6029.

3 G. Mathis, *Clin. Chem.*, 1993, **39**, 1953; 1995, **41**, 1391; E. Lopez, C. Chypre, B. Alpha and G. Mathis, *Clin. Chem.*, 1993, **39**, 196; N. Sabbatini, M. Guardigli, I. Manet, R. Ungaro, A. Casnati, R. Ziessel, G. Ulrich, Z. Asfari and J.-M. Lehn, *Pure Appl. Chem.*, 1995, **67**, 135; H. Takalo, I. Hemmilä, T. Sutela and M. Latva, *Helv. Chim. Acta*, 1996, **79**, 789.

4 S. Aime, M. Botta, D. Parker and J. A. G. Williams, *J. Chem. Soc., Dalton Trans.*, 1996, 17; 1995, 2259; D. H. Powell, M. Favre, N. Graeppi, O. M. Ni Dhubhghaill, D. Pubanz and A. E. Merbach, *J. Alloys Compd.*, 1995, **225**, 246; K. Kumar and M. F. Tweedle, *Pure Appl. Chem.*, 1993, **65**, 515; R. B. Lauffer, *Chem. Rev.*, 1987, **87**, 901.

5 C. Piguet and J.-C. G. Bünzli, *Eur. J. Solid State Inorg. Chem.*, 1996, **33**, 165.

6 C. Piguet, J.-C. G. Bünzli, G. Bernardinelli, G. Hopfgartner and A. F. Williams, *J. Alloy Compd.*, 1995, **225**, 324; C. Piguet, *Chimia*, 1996, **50**, 144.

7 F. W. Lichtenhaler, *Angew. Chem., Int. Ed. Engl.*, 1994, **33**, 2364.

8 V. Alexander, *Chem. Rev.*, 1995, **95**, 273; P. Guerriero, S. Tamburini and P. A. Vigato, *Coord. Chem. Rev.*, 1995, **139**, 17.

9 N. Sabbatini, M. Guardigli and J.-M. Lehn, *Coord. Chem. Rev.*, 1993, **123**, 201.

10 J.-M. Lehn and J.-B. Regnouf de Vains, *Helv. Chim. Acta*, 1992, **75**, 1221; J.-M. Lehn, *Angew. Chem., Int. Ed. Engl.*, 1988, **27**, 89; P. H. Smith, Z. E. Reyes, C. W. Lee and K. N. Raymond, *Inorg. Chem.*, 1988, **27**, 4154.

11 L. W. Yang, S. Liu, E. Wong, S. J. Rettig and C. Orvig, *Inorg. Chem.*, 1995, **34**, 2164; P. Caravan, T. Hedlund, S. Liu, S. Sjöberg and C. Orvig, *J. Am. Chem. Soc.*, 1995, **117**, 11230; V. Balzani, E. Berghmans, J.-M. Lehn, N. Sabbatini, R. Terörde and R. Ziessel, *Helv. Chim. Acta*, 1990, **73**, 2083; R. Ziessel, M. Maestri, L. Prodi, V. Balzani and A. Van Doersselaer, *Inorg. Chem.*, 1993, **32**, 1237; N. Sabbatini, M. Guardigli, I. Manet, F. Bolleta and R. Ziessel, *Inorg. Chem.*, 1994, **33**, 955; J. Xu, S. J. Franklin, D. W. Whisenhunt and K. N. Raymond, *J. Am. Chem. Soc.*, 1995, **117**, 7245.

12 B. Dietrich, P. Viout and J.-M. Lehn, *Macrocyclic Chemistry*, VCH, Weinheim, New York, Basel and Cambridge, 1992.

13 D. A. Koshland, *Angew. Chem., Int. Ed. Engl.*, 1994, **33**, 2375.

14 D. A. Durham, G. H. Frost and F. A. Hart, *Chem. Commun.*, 1969, 1421; G. H. Frost, F. A. Hart and M. B. Hursthouse, *J. Inorg. Nucl. Chem.*, 1969, **31**, 831.

15 C. Piguet, A. F. Williams, G. Bernardinelli and J.-C. G. Bünzli, *Inorg. Chem.*, 1993, **32**, 4139.

16 C. Piguet, J.-C. G. Bünzli, G. Bernardinelli, C. G. Bochet and P. Froidevaux, *J. Chem. Soc., Dalton Trans.*, 1995, 83.

17 C. Piguet, G. Hopfgartner, A. F. Williams and J.-C. G. Bünzli, *J. Chem. Soc., Chem. Commun.*, 1995, 491; C. Piguet, E. Rivara-Minten, G. Hopfgartner and J.-C. G. Bünzli, *Helv. Chim. Acta*, 1995, **78**, 1541.

18 C. Piguet, E. Rivara-Minten, G. Hopfgartner and J.-C. G. Bünzli, *Helv. Chim. Acta*, 1995, **78**, 1651.

19 C. Piguet, G. Bernardinelli, J.-C. G. Bünzli, S. Petoud and G. Hopfgartner, *J. Chem. Soc., Chem. Commun.*, 1995, 2575.

20 C. Piguet, J.-C. G. Bünzli, G. Bernardinelli, G. Hopfgartner, S. Petoud and O. Schaad, *J. Am. Chem. Soc.*, 1996, **118**, 6681.

21 F. A. Cotton and G. Wilkinson, *Advanced Inorganic Chemistry*, 3rd edn., Interscience, New York, London, Sydney, Toronto, 1972, p. 862.

22 H. Toftlund, *Coord. Chem. Rev.*, 1989, **94**, 67.

23 O. Kahn and J. P. Launay, *Chemtronics*, 1988, **3**, 140.

24 O. Kahn and E. Codjovi, *Philos. Trans. R. Soc. London, Ser. A*, 1996, **354**, 359.

25 C. Piguet, G. Hopfgartner, B. Bocquet, O. Schaad and A. F. Williams, *J. Am. Chem. Soc.*, 1994, **116**, 9092.

26 G. Hopfgartner, C. Piguet, J. D. Henion and A. F. Williams, *Helv. Chim. Acta*, 1993, **76**, 1789; G. Hopfgartner, C. Piguet and J. D. Henion, *J. Am. Soc. Mass Spectrom.*, 1994, **5**, 748; F. M. Romeo, R. Ziessel, A. Dupont-Gervais and A. van Dorsselaer, *Chem. Commun.*, 1996, 551.

27 A. Marquis-Rigault, A. Dupont-Gervais, P. N. W. Baxter, A. van Dorsselaer and J.-M. Lehn, *Inorg. Chem.*, 1996, **35**, 2307; E. Leize, A. van Dosselaer, R. Krämer and J.-M. Lehn, *J. Chem. Soc., Chem. Commun.*, 1993, 990.

28 E. R. Malinowski and D. G. Howery, *Factor Analysis in Chemistry*, Wiley, New York, Chichester, Brisbane, Toronto, 1980.

29 C. Piguet, G. Bernardinelli, B. Bocquet, A. Quattropani and A. F. Williams, *J. Am. Chem. Soc.*, 1992, **114**, 7440.

30 J. Polster and H. Lachmann, *Spectrometric Titrations, Analysis of Chemical Equilibria*, VCH, Weinheim, Basel, Cambridge, New York, 1989.

31 P. Krumholz, *Struct. Bond.* (*Berlin*), 1971, **9**, 139.

32 K. A. Reeder, E. V. Dose and L. J. Wilson, *Inorg. Chem.*, 1978, **17**, 1071.

33 P. Lainé, A. Gourdon and J.-P. Launay, *Inorg. Chem.*, 1995, **34**, 5129.

34 M. T. Youinou, R. Ziessel and J.-M. Lehn, *Inorg. Chem.*, 1991, **30**, 2144.

35 G. R. Choppin in *Lanthanide Probes in Life, Chemical and Earth Sciences*, eds. J.-C. G. Bünzli and G. R. Choppin, Elsevier, Amsterdam, 1989, ch. 1.

36 P. S. Braterman, J. I. Song and R. D. Peacock, *Inorg. Chem.*, 1992, **31**, 555.

37 J. Massaux and G. Duyckaerts, *Anal. Chim. Acta*, 1974, **73**, 416.

38 P. H. Smith, Z. E. Reyes, C. N. Lee and K. N. Raymond, *Inorg. Chem.*, 1988, **27**, 4154.

39 S. Petoud, J.-C. G. Bünzli, F. Renaud and C. Piguet, *J. Alloys Compd.*, in the press.

40 S. Rüttimann, C. Piguet, G. Bernardinelli, B. Bocquet and A. F. Williams, *J. Am. Chem. Soc.*, 1992, **114**, 4230.

41 P. D. Burns and G. N. La Mar, *J. Magn. Reson.*, 1982, **46**, 61.

42 I. Bertini and C. Luchinat, *NMR of Paramagnetic Molecules in Biological Systems*, Benjamin/Cummings Publishing Co., Menlo Park, CA, 1986.

43 P. Gütlich, A. Hauser and H. Spiering, *Angew. Chem., Int. Ed. Engl.*, 1994, **33**, 2024.

44 R. D. Shannon, *Acta Crystallogr. Sect. A*, 1976, **32**, 751.

45 O. Kahn, *Molecular Magnetism*, VCH, Weinheim, 1993.

46 D. F. Evans, *J. Chem. Soc.*, 1959, 2003; T. H. Crawford and

J. Swanson, *J. Chem. Educ.*, 1971, **48**, 382; J. Löliger and R. Sheffold, *J. Chem. Educ.*, 1972, **49**, 646.

47 M. V. Baker, L. D. Field and T. W. Hambley, *Inorg. Chem.*, 1988, **27**, 2872.

48 D. H. Grant, *J. Chem. Educ.*, 1995, **72**, 39.

49 C. Piguet, *J. Chem. Educ.*, in the press.

50 K. H. Sugiyarto, D. C. Craig, D. A. Rae and H. A. Goodwin, *Aust. J. Chem.*, 1994, **47**, 869.

51 A. Bouayad, C. Brouca-Cabarrecq and J.-C. Trombe, *Inorg. Chim. Acta*, 1992, **195**, 193; C. Benelli, A. Caneschi, D. Gatteschi, O. Guillou and L. Prodi, *Inorg. Chem.*, 1990, **29**, 1750.

52 C. Benelli, A. J. Blake, P. E. Y. Milne, J. M. Rawson and R. E. P. Winpenny, *Chem. Eur. J.*, 1995, **1**, 614.

53 L. Chen, S. R. Breeze, R. J. Rousseau, S. Wang and L. K. Thompson, *Inorg. Chem.*, 1995, **34**, 454.

54 K. H. Sugiyarto, D. C. Craig, D. A. Rae and H. A. Goodwin, *Aust. J. Chem.*, 1995, **48**, 35.

55 C. K. Johnson, ORTEP II, Report ORNL-5138, Oak Ridge National Laboratory, Oak Ridge, TN, 1976.

56 J. M. Harrowfield, Y. Kim, B. W. Skelton and A. H. White, *Aust. J. Chem.*, 1995, **48**, 807.

57 C. Piguet, G. Bernardinelli, B. Bocquet, O. Schaad and A. F. Williams, *Inorg. Chem.*, 1994, **33**, 4112.

58 L. G. Vanquickenborne and K. Pierloot, *Inorg. Chem.*, 1981, **20**, 3673.

59 J.-M. Lehn, *Angew. Chem., Int. Ed. Engl.*, 1990, **29**, 1304.

60 J. F. Desreux, in *Lanthanide Probes in Life, Chemical and Earth Sciences*, eds. J.-C. G. Bünzli and G. R. Choppin, Elsevier, Amsterdam, 1989, ch. 2, p. 43.

61 W. C. Wolsey, *J. Chem. Educ.*, 1973, **55**, A355.

62 E. Blanc, D. Schwarzenbach and H. D. Flack, *J. Appl. Crystallogr.*, 1991, **24**, 1035.

63 P. Main, S. J. Fiske, S. E. Hull, L. Lessinger, D. Germain, J. P. Declercq and M. M. Woolfson, MULTAN 87, Universities of York and Louvain-La-Neuve, 1987.

64 *XTAL 3.2 User's Manual*, eds. S. R. Hall and J. M. Stewart, Universities of Western Australia and Maryland, 1989.

65 C. Piguet, A. F. Williams, G. Bernardinelli, E. Moret and J.-C. G. Bünzli, *Helv. Chim. Acta*, 1992, **75**, 1697.

66 A. J. Bard and L. R. Faulkner, *Electrochemical Methods, Fundamentals and Application*, Wiley, New York, Chichester, Brisbane, Toronto, Singapore, 1980.

67 D. S. Raiford, C. L. Fisk and E. D. Becker, *Anal. Chem.*, 1979, **51**, 2050.

68 D. Ostfeld and I. A. Cohen, *J. Chem. Educ.*, 1972, **49**, 829; R. F. Brunel and K. V. Bibber, *International Critical Tables*, McGraw-Hill, New York, London, 1930.

69 T. P. Abeles and W. G. Bos, *J. Chem. Educ.*, 1967, **44**, 438.